Journal of Neuroinflammation

RESEARCH

Open Access

Inhibition of EED-mediated histone methylation alleviates neuroinflammation by suppressing WNT-mediated dendritic cell migration

Wenxiang Hong[1,2†], Hongbo Ma[1†], Zhibin Li[1,3], Yiwen Du[1], Wenjing Xia[1], Han Yin[1], Han Huang[1], Zebing Sun[1], Renhua Gai[1], Lexian Tong[2], Hong Zhu[1,2], Jincheng Wang[1,3,4], Bo Yang[1,5], Qiaojun He[1,6], Qinjie Weng[1,4,5,6*] and Jiajia Wang[1,2,3*]

Abstract

The epigenetic modification of histone H3 lysine 27 trimethylation (H3K27me3) by the embryonic ectoderm development (EED) protein is closely associated with the regulation of transcriptional programs and is implicated in autoimmune diseases. However, the efficacy of targeting H3K27me3 for the treatment of neuroinflammation remains unclear. In this study, we demonstrate that systemic administration of an EED inhibitor diminishes the inflammatory response mediated by dendritic cells (DCs), thereby alleviating experimental autoimmune encephalitis (EAE), a representative mouse model of autoimmune diseases in the central nervous system (CNS). Our findings indicate that EED inhibitors suppress DC migration by upregulating genes in the WNT signaling pathway that are epigenetically marked by H3K27me3. Conversely, inhibiting the WNT pathway partially reverses the impaired DC migration caused by EED inhibitors. Additionally, the genetic deletion of *Eed* inhibits DC migration and effectively mitigates autoimmune symptoms and inflammatory infiltration into the CNS in EAE. These results highlight EED as a critical regulator of DC migration and suggest its potential as a therapeutic target for autoimmune disorders.

Keywords Autoimmune diseases, Neuroinflammation, Dendritic cells, Migration, H3K27me3, WNT

†Wenxiang Hong and Hongbo Ma contributed equally to this work.

*Correspondence:
Qinjie Weng
wengqinjie@zju.edu.cn
Jiajia Wang
wangjiajia3301@zju.edu.cn
[1] Center for Drug Safety Evaluation and Research, Zhejiang Province Key Laboratory of Anti-Cancer Drug Research, College of Pharmaceutical Sciences, Zhejiang University, Hangzhou 310058, China
[2] Innovation Institute for Artificial Intelligence in Medicine of Zhejiang University, Hangzhou 310018, China
[3] Hangzhou Institute of Innovative Medicine, College of Pharmaceutical Sciences, Zhejiang University, Hangzhou 310058, China
[4] Taizhou Institute of Zhejiang University, Zhejiang University, Taizhou 318000, China
[5] Institute of Fundamental and Transdisciplinary Research Zhejiang University, Zhejiang University, Hangzhou 310058, China
[6] The Second Affiliated Hospital, Zhejiang University School of Medicine, Hangzhou 310009, China

Introduction

Histone modifications, which are followed with alterations in chromatin reorganization and genetic transcription, are pivotal events essential for vertebrate development [1, 2]. The trimethylation of histone H3 lysine K27 (H3K27me3) is a well-established mark that plays a critical role in chromatin compaction and transcriptional repression [3–5]. The polycomb repressive complex 2 (PRC2), which is the sole complex that catalyzes H3K27me3, comprises three core subunits: the methyltransferase EZH2 (enhancer of zeste homolog 2), which acts as a "writer" of the methylation mark, the methyl group-binding EED (embryonic ectoderm development) subunit, which serves as a "reader" of methylated H3K27, and the SUZ12 (suppressor of zeste 12) [3–5]. The development of small molecule inhibitors that target these epigenetic regulators has shown great promise in disease intervention, especially with the commercial availability of the EZH2 inhibitor Tazemetostat and the ongoing clinical trials for several allosteric EED inhibitors [6]. However, the majority of research and clinical trials have concentrated on cancer treatment, and the potential roles of these inhibitors in other diseases are not yet fully understood [6, 7].

Accumulating evidence suggests that H3K27me3 plays fundamental roles in autoimmune diseases in the central nervous system (CNS), such as multiple sclerosis (MS). MS is a chronic, neurodegenerative disorder that is primarily characterized by demyelination, axonal loss, and multifocal inflammation within the CNS [8, 9]. A reduction in EZH2 expression has been noted in peripheral blood mononuclear cells from MS patients compared to that from controls [10]. Network-based analysis reveals that EED and EZH2 genes in cerebrospinal fluid are identified as potential candidate genes for MS therapy [11]. Although the overall genome-wide H3K27me3 levels don't differ significantly in $CD4^+$ T cells from WT and experimental allergic encephalomyelitis (EAE) mice, a well-established mouse model of MS, the intensity of the histone marks in certain genomic regions is significantly altered in EAE mice [12, 13]. Notably, *Ezh2* deficiency in macrophages is able to inhibit H3K27me3 and stimulate the expression of anti-inflammatory gene *Socs3*, thus hindering autoimmune inflammation of EAE [12, 13]. Thus, PRC2/H3K27me3 may accelerate inflammation in MS and be a potential target for disease intervention.

However, the role of PRC2 components or H3K27me3 varies across different immune cells. For instance, *Ezh2* deficiency in dendritic cells (DCs) impairs integrin-dependent transendothelial migration and reduces inflammation in EAE mice, but in a manner that is independent of H3K27me3 [14]. In contrast, *Suz12* depletion in DCs significantly reduces their ability to maintain H3K27me3 levels, yet it does not affect their development or the efficiency of their immune responses [15]. On the other hand, T cells with *Eed* deficiency show an impaired response to TGF-β in vitro, leading to decreased induction of FOXP3 expression and increased expression of molecules associated with non-Treg cell differentiation, such as Runx3 in $CD8^+$ cells, which exacerbates inflammation [16, 17]. Furthermore, Zbtb46 and HSP70L1 contribute to the maintenance of repressive H3K27me3 marks in costimulatory and major histocompatibility complex (MHC) molecules, thereby inhibiting DC maturation [18, 19]. Taken together, the complex role of PRC2 and H3K27me3 in EAE is not fully understood and warrants further investigation.

Herein, we demonstrated that EED inhibitors not only block DC migration but also mitigate the inflammatory response in an EAE mouse model, suggesting significant therapeutic potential for neuroinflammatory diseases. By generating *Eed* conditional knockout mice, we further discovered that treatment with EED inhibitors upregulates WNT signaling pathway genes, which are targeted by H3K27me3 in DCs. Inhibition of the WNT pathway can partially reverse the impaired DC migration caused by EED inhibitors. Additionally, the inhibitory effect of EED inhibitors on DC migration was confirmed in human DCs. Thus, our findings uncover a previously unidentified role of EED in epigenetic regulation of DC migration and EAE prevention, offering a promising new avenue for autoimmune diseases therapy.

Results

Mice treated with EED inhibitors are refractory to the development of EAE

Considering the complex and inconsistent roles of PRC2 or H3K27me3 in the pathogenesis of EAE and multiple immune cells, the precise contribution of H3K27me3 to EAE development remains to be elucidated. In this study, we delve into the impact of EED226, an EED inhibitor that can reduce H3K27me3 levels, on both the progression and inflammatory pathology of EAE. EED226 was administrated at a dosage of 40 mg/kg, twice daily, in an EAE mouse model (Fig. 1A). The clinical signs of EAE, including tail tip, hindlimb, and forelimb paralysis, typically emerged by day 8 post-immunization (dpi 8), and peaked from dpi 21 to dpi 30. Notably, EED226 treatment resulted in a significant attenuation of disease sensitivity and a marked alleviation of symptoms throughout the disease progression (Fig. 1B). Expectedly, hematoxylin and eosin (H&E) staining demonstrated a robust suppression of inflammatory infiltration in the demyelinated regions after EED226 treatment (Fig. 1C). Luxol fast blue (LFB) and electron microscopy analysis indicated that EED226-treated EAE mice exhibited a more preserved

myelin sheath in the damaged lumbar spinal cord compared to vehicle-treated EAE mice (Fig. 1C–E). These data underscored the protective effect of EED226 in the EAE mouse model.

Given the key role of T cells in the immune responses associated with MS [9, 20], our study sought to delineate the modification in T cell activation induced by EED226 treatment in EAE mice using flow cytometry. Results showed that EED226 treatment significantly expanded the population of $CD4^+CD62L^{hi}CD44^{lo}$ naive T cells and concurrently reduced the proportion of $CD4^+CD62L^{lo}CD44^{hi}$ central memory T cells (Fig. 1F). Additionally, the differentiation of pro-inflammatory Th1 ($CD4^+IFN\text{-}\gamma^+$) and Th17 ($CD4^+IL\text{-}17^+$) subsets was markedly suppressed following EED226 administration in EAE mice (Fig. 1G). Antigen presenting cells, particularly DCs, are well-established for their capacity to capture antigens, migrate to lymph nodes or the spleen, and present antigens to T cells, thereby initiating and amplifying inflammation and myelin damage in MS [21, 22]. Notably, flow cytometry analysis revealed a significant reduction in the percentage of migratory $CD11c^+$ DCs within splenic cells following EED226 administration (Fig. 1H), as well as the proportion of mature DCs, identified by $CD11c^+CD80^+$ or $CD11c^+MHC\text{-}II^+$ markers (Fig. 1I). However, the ratio of $CD80^+$ or $MHC\text{-}II^+$ mature DCs within the total $CD11c^+$ DC population remained comparable between vehicle and EED226-treated EAE mice (Fig. 1J), suggesting a critical role for EED inhibitors in modulating DC migration rather than maturation in the context of EAE. Altogether, these results underscored the inhibitory effect of EED226 on immune activation, thereby conferring resistance to EAE development.

EED inhibitors restrain DC migration in an EED-dependent way

Expanding upon the aforementioned findings, we proceeded to examine the inhibitory effects of EED inhibitors on cultured DCs. A panel of EED inhibitors, including A395, MAK683, EEDi-5285, and EED226, was incubated with the mouse dendritic cell line DC2.4. A survival assay revealed no significant cytotoxicity at the concentrations up to 10 μM for these EED inhibitors (Fig. 2A). Given that these inhibitors primarily bind to the H3K27me3-binding pocket of EED and then prevent allosteric activation of the catalytic activity of EED [7, 23–25], subsequent western blotting analysis confirmed the effective reduction of H3K27me3 levels but not EED protein by A395, MAK683, and EEDi-5285 at 5 μM, and by EED226 at 10 μM (Fig. 2B). To assess the impact of EED inhibitors on DC migration, we then conducted an in vitro transwell assay coupled with crystal violet staining, in response to the chemokines CCL19 and CCL21 [26], which are pivotal for mature DC migration (Fig. 2C). The results demonstrated a significant inhibition of DC migration from the upper to the lower chamber in the presence of EED inhibitors (Fig. 2D). Besides, our immunofluorescence assays showed that F-actin cytoskeleton, which is typically polarized or dispersed near the cell surface or antennae for the extension of the pseudopods and DC migration [26, 27], was predominantly localized near the nucleus in both control and EED inhibitor-treated DC2.4 cells (Fig. 2E), indicating that EED inhibitors restricted the formation of pseudopods in DCs. Moreover, EED overexpression partially reversed the suppressive effects of these inhibitors on H3K27me3 expression and DC migration, suggesting that their functionality is at least partially mediated through EED (Fig. 2F–H). Collectively, these findings depicted a potent suppression of DC migration by EED inhibitors.

EED inhibitors regulate the transcriptional program necessary for DC migration

To understand the molecular mechanism by which EED inhibitors regulate DC migration, we subjected LPS-induced DC2.4 cells to treatment with either vehicle or

(See figure on next page.)

Fig. 1 EED226 ameliorates symptoms and inflammation in EAE mice. **A** Scheme for the induction, assessment and drug administration of EAE mice. **B** Clinical scores of vehicle or EED226 treated EAE mice. $n = 10$ animals, 5 animals are sacrificed for the histopathological examination and flow cytometry analysis at day 22 post immunization (dpi 22). * indicates a statistically difference when compared with EAE + vehicle group. **C** Representative images of H&E staining (top) and LFB staining (bottom) for spinal cords from vehicle or EED226 treated EAE mice at dpi 22. Scale bar: 50 μm. $n = 3$. **D** Bar graph for LFB staining analysis of the demyelinated area in the spinal cords of vehicle or EED226 treated EAE mice at dpi 22. $n = 3$. **E** Representative images (left) and bar graph (right) for electron microscopy analysis of the demyelination in the spinal cords of vehicle or EED226 treated EAE mice at dpi 22. Scale bar: 2 μm. $n = 3$. **F** Representative images (left) and bar graph (right) for flow cytometry analysis of the frequency of naïve T cells ($CD4^+CD62L^{hi}CD44^{lo}$) and central memory T cells ($CD4^+CD62L^{lo}CD44^{hi}$) in the spleen of vehicle or EED226 treated EAE mice at dpi 22. $n = 3$. **G** Representative images (left) and bar graph (right) for flow cytometry analysis of the frequency of Th1 ($CD4^+IFN\text{-}\gamma^+$) and Th17 ($CD4^+IL\text{-}17^+$) in the spleen of vehicle or EED226 treated EAE mice at dpi 22. $n = 3$. **H** Representative images (left) and bar graph (right) for flow cytometry analysis of the frequency of total DCs ($CD11c^+$) in the spleen of vehicle or EED226 treated EAE mice at dpi 22. $n = 3$. **I** Representative images (left) and bar graph (right) for flow cytometry analysis of the frequency of mature DCs ($CD11c^+CD80^+$, $CD11c^+MHC\text{-}II^+$) in the spleen of vehicle or EED226 treated EAE mice at dpi 22. $n = 3$. **J** Bar graph for flow cytometry analysis of the percentage of $CD80^+$ or $MHC\text{-}II^+$ in $CD11c^+$ DCs in the spleen of vehicle or EED226 treated EAE mice at dpi 22. $n = 3$. Data are presented as mean ± SD. *, $P < 0.05$; **, $P < 0.01$; ***, $P < 0.001$; ns, not significant

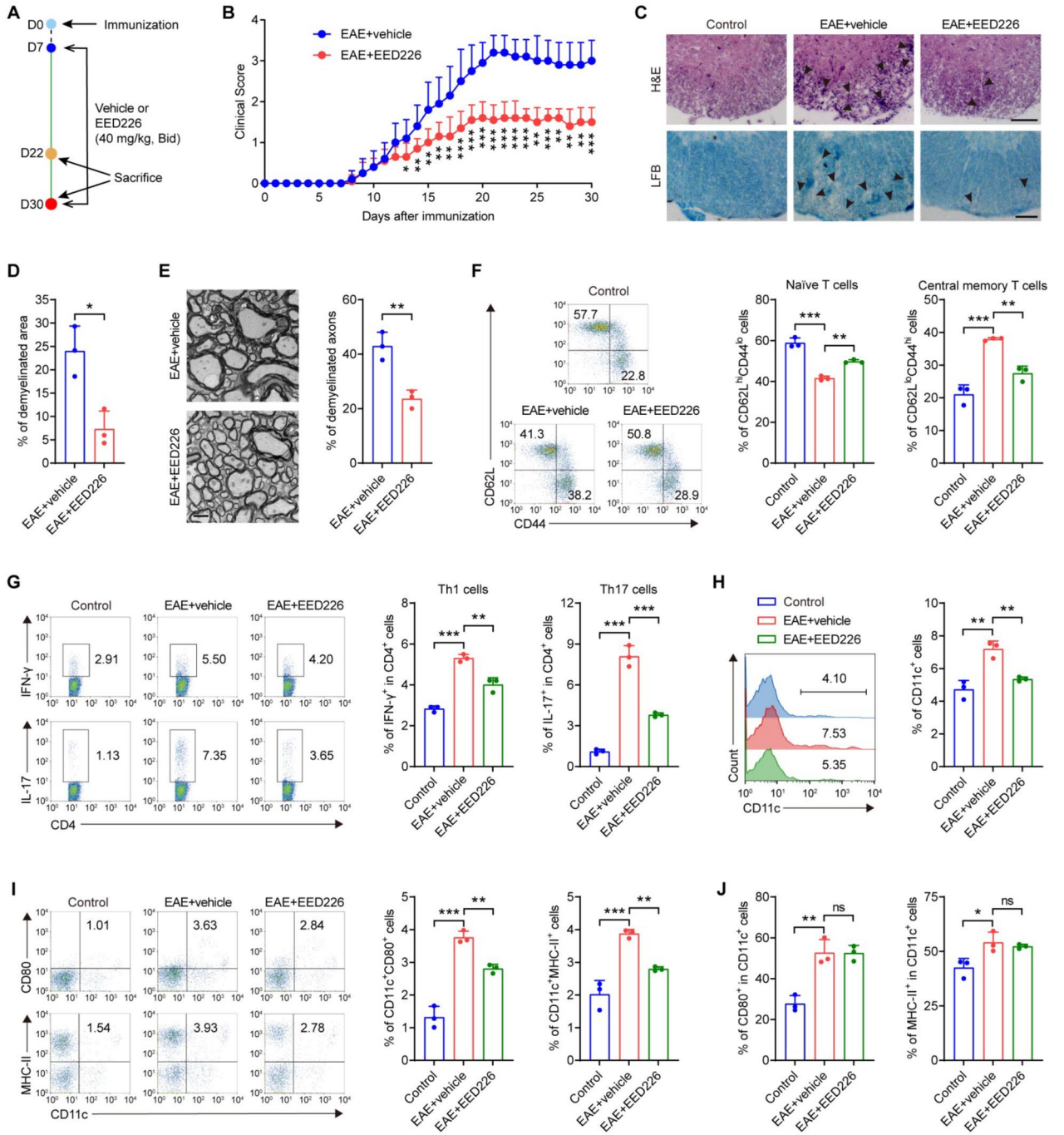

Fig. 1 (See legend on previous page.)

EEDi-5285, an EED inhibitor, and performed transcriptome profiling. Principal components analysis (PCA) distinctly segregated the transcriptomes of the vehicle and EEDi-5285 groups (Fig. 3A). Further analysis using a volcano plot and heatmap identified a cohort of differentially expressed genes (fold change > 2, $P < 0.05$) between the EEDi-5285 and vehicle groups, comprising 565 genes that were significantly upregulated and 156 that were significantly downregulated in EEDi-5285 group (Fig. 3B, C). These findings are consistent with the anticipated outcome, given that the inhibition of EED-regulated H3K27me3 is associated with transcriptional de-repression [4], leading to the activation of a multitude of genes.

Furthermore, Gene Set Enrichment Analysis (GSEA) uncovered that the genes significantly downregulated in the EEDi-5285 group were predominantly enriched in gene signatures related to inflammatory response, microtubule cytoskeleton organization, NF-κB activation, and Rho GTPases activate formins. Conversely, gene signatures associated with the negative chemotaxis, negative regulation of inflammatory response, negative regulation of blood vessel endothelial cell migration, and TGF-β1 signaling were enriched in the EEDi-5285 group, all of which are implicated in the migratory behavior of DCs (Fig. 3D). In consistence, genes pertinent to DC migration, such as *Ccl9*, *Ccr7*, *Itgb7*, *Rhoa*, *Ripor2*, *Tubb6*, and *Cxcl2* exhibited reduced expression levels in the EEDi-5285 group (Fig. 3E), thereby further corroborating the inhibitory effects of EED inhibitors on DC migration.

EED inhibitors suppress H3K27me3, thereby augmenting the WNT signaling pathway to repress DC migration

Given that EED functions as an epigenetic reader for the H3K27me3 mark, GSEA uncovered that genes upregulated in the EEDi-5285 group were enriched in gene signatures associated with H3K27me3 targets, EED targets and PRC2 targets (Fig. 3F–H). Notably, the expression levels of classical H3K27me3 target genes, such as *Wnt7b*, *Trp53i11*, and *Lef1*, were elevated in EEDi-5285 treated DC2.4 cells (Fig. 3I). To delineate genes directly targeted by the EED/H3K27me3 in DCs, an analysis of H3K27me3 ChIP-seq data from human DCs was conducted [28]. The H3K27me3 peak signals were predominantly localized near the transcriptional start sites (TSS) in human DCs (Fig. 4A). Integration of ChIP-seq with RNA-seq data identified 431 genes with significant upregulation and H3K27me3 deposition (Fig. 4B), further substantiating the role of H3K27me3 following EEDi-5285 treatment. Kyoto Encyclopedia of Genes and Genomes (KEGG) and transcriptome analyses highlighted that pathways including WNT, Hippo, Calcium, PI3K-AKT, and Rap1 were notably enriched and activated within the 431 overlapped genes after EED inhibitor intervention (Fig. 4C, D).

Interestingly, differentially expressed genes with high H3K27me3 occupancy in EEDi-5285-treated DCs, such as *Wnt6*, *Frzb*, and *Sfrp2*, were found predominantly associated with the WNT pathway (Fig. 4E, F). This implicated the WNT signaling pathway as a pivotal mediator of H3K27me3 effects in DCs modulated by EED inhibitors. GSEA substantiated the significant enrichment of the WNT/β-catenin signaling cascade in DC2.4 cells exposed to EEDi-5285 (Fig. 4G). qRT-PCR corroborated the induction of WNT/β-catenin-responsive genes, including *Wnt5a*, *Wnt10a*, *Frzb*, *Sfrp2*, and *Sfrp1*, following treatment with a panel of EED inhibitors (Fig. 4H). However, these EED inhibitors lost their capacity to inhibit DC migration upon treatment with WNT signaling inhibitor Wnt-C59, indicating WNT signaling activation was responsible for EED's regulation of DC migration (Fig. 4I). In brief, our results delineated a novel regulatory mechanism whereby EED inhibitors enhance WNT signaling to stamp down DC migration.

Eed deficiency intercepts DC migration via WNT signaling

The impact of EED inhibitors on DC migration has implications for immune activation and the pathogenesis of EAE, suggesting the potential of EED as a therapeutic target for autoimmune diseases. To ascertain the specific effects of EED in DC regulation, we genetically deleted *Eed* in DCs by crossing *Eed*-floxed mice with mice expressing the *CD11c*-Cre driver specifically in DCs (Fig. 5A). We then isolated and cultured murine bone marrow-derived dendritic cells (BMDCs) from the resulting conditional *Eed* knockout mice (*Eed* $^{flox/flox}$; *CD11c*-Cre mice, hereafter referred to as *Eed* cKO) and their littermate controls. Western blotting analysis confirmed the successful ablation of EED and the consequent reduction of H3K27me3 in *Eed* cKO BMDCs (Fig. 5B). Flow cytometry analysis revealed negligible effects of *Eed*

(See figure on next page.)

Fig. 2 EED inhibitors impair the migration of DC2.4 cells. **A** SRB analysis for the survival rate of DC2.4 upon treatment with different EED inhibitors at various concentrations (0, 0.32, 0.63, 1.25, 2.5, 5, 10, 20 or 40 μM) for 24 h. $n = 3$. * indicates a statistically difference when compared with 0 μM. **B** Western blotting analysis (left) and corresponding quantification (right) for the expression of H3K27me3 and EED in DC2.4 after treatment with A395 (5 μM), MAK683 (5 μM), EEDi-5285 (5 μM) or EED226 (10 μM) for 24 h. $n = 3$. **C** Scheme for transwell analysis of chemokines-triggered migration of DC2.4 after treating with LPS or different EED inhibitors. **D** Representative images (left) and statistics (right) for transwell analysis together with crystal violet staining in DC2.4 after treating with A395 (5 μM), MAK683 (5 μM), EEDi-5285 (5 μM) or EED226 (10 μM) for 24 h and LPS (50 ng/mL) for 6 h. Scale bar: 200 μm. $n = 3$. **E** Immunostaining of F-Actin (green) in DC2.4 after treating with A395 (5 μM), MAK683 (5 μM), EEDi-5285 (5 μM) or EED226 (10 μM) for 24 h and LPS (50 ng/mL) for 6 h. Scale bar: 10 μm. $n = 3$. **F** Western blotting analysis (left) and the corresponding quantification (right) for the expression of H3K27me3 in DC2.4 after transfection with HA-EED plasmid and treatment with A395 (5 μM), MAK683 (5 μM), EEDi-5285 (5 μM) or EED226 (10 μM) for 24 h and LPS (50 ng/mL) for 6 h. $n = 3$. **G** Scheme for transwell analysis of chemokines-triggered migration of DC2.4 after transfection with HA-EED plasmid and treatment with LPS and EED inhibitors. **H** Representative images (left) and statistics (right) for transwell analysis together with crystal violet staining in DC2.4 cells after transfection with HA-EED plasmid and treatment with A395 (5 μM), MAK683 (5 μM), EEDi-5285 (5 μM) or EED226 (10 μM) for 24 h and LPS (50 ng/mL) for 6 h. Scale bar: 200 μm. $n = 3$. Data are presented as mean ± SD. *, $P < 0.05$; **, $P < 0.01$; ***, $P < 0.001$; ns, not significant

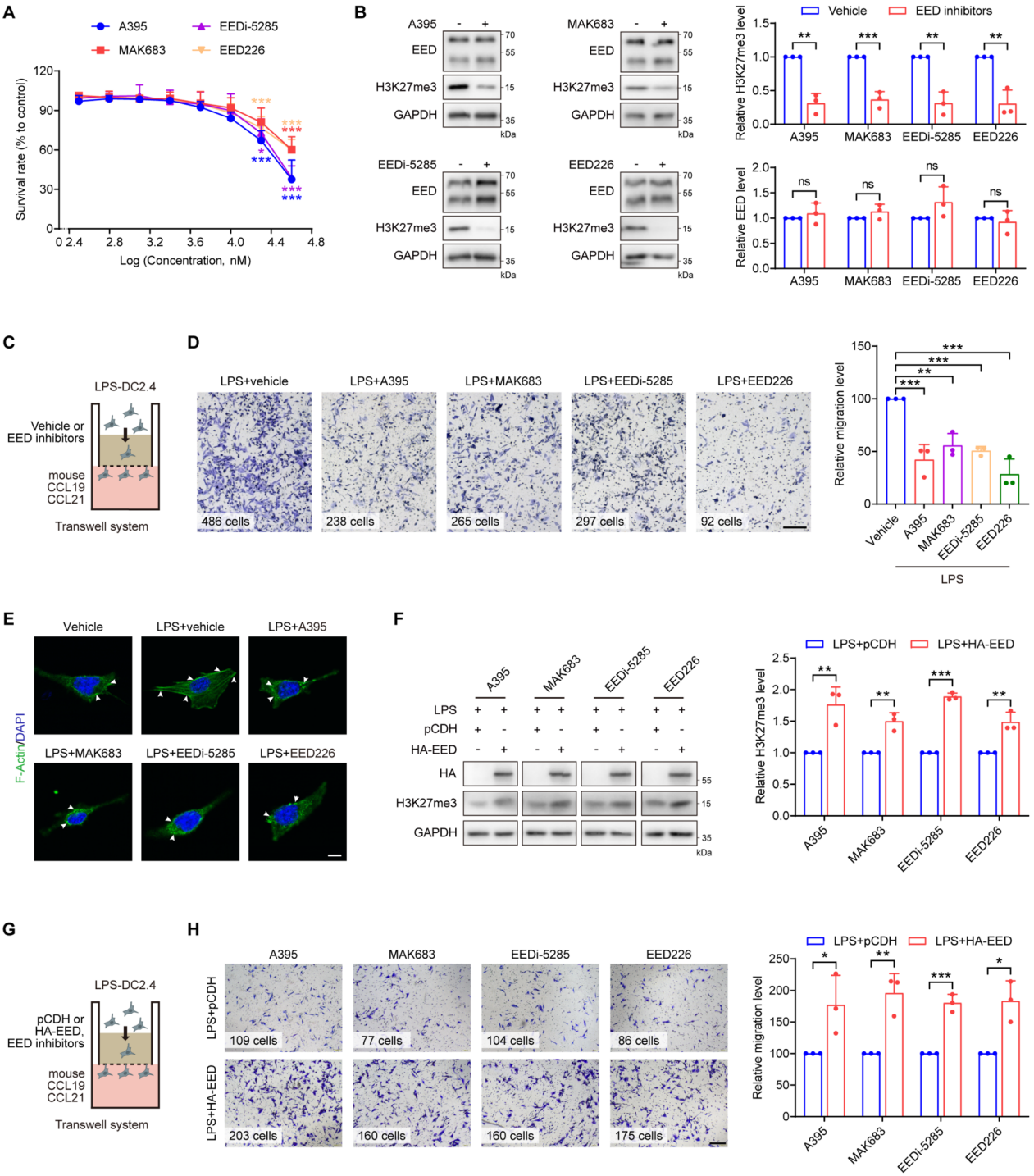

Fig. 2 (See legend on previous page.)

deficiency on the successful differentiation of bone marrow cells into DCs (Fig. 5C, D). Additionally, *Eed* knockout had minimal impact on DC maturation, as evidenced by the largely unchanged proportions and numbers of $CD80^+$, $CD86^+$ or $MHC\text{-}II^+$ cells in BMDCs (Fig. 5E, F).

Transwell assays revealed that *Eed* ablation significantly inhibited DC migration in response to CCL19 and CCL21 chemokines, and treatment with EED inhibitors did not further decrease cell migration, suggesting that the effects of EED inhibitors are EED-dependent

(Fig. 5G). It has been reported DC cytoskeletal rearrangement is required for the formation of its immunological synapse. Besides, the inhibition of cell migration or motility can reduce cell-to-cell contact within the confined space of co-culture systems [29–32]. Both of which are necessary for DC activation of T cell proliferation. As expected, *Eed* deficiency significantly inhibited DC-induced differentiation of T cells into pro-inflammatory Th1 ($CD4^+IFN\text{-}\gamma^+$) and Th17 ($CD4^+IL\text{-}17^+$) subsets upon stimulation with LPS and $MOG_{35\text{-}55}$ peptide (Fig. 5H). Consistent with the effects of EED inhibitors, qRT-PCR analysis revealed an upregulation of mRNA levels for genes involved in the WNT/β-catenin pathway, such as *Wnt6*, *Wnt5a*, and *Sfrp2*, in BMDCs derived from *Eed* cKO mice (Fig. 5I). Further, CUT&Tag-qPCR results showed that H3K27me3 enrichment in the promoters of WNT target genes, like *Wnt6*, *Wnt5a*, and *Wnt10a*, was reduced significantly after *Eed* deletion, indicating that EED directly regulates expression of these genes in BMDCs (Fig. 5J). Moreover, treatment with Wnt-C59 successfully reversed the reduced cell migration observed in *Eed* cKO BMDCs (Fig. 5K), further supporting the necessity of EED for DC migration via WNT signaling.

Eed deficiency in DC alleviates EAE development

Subsequently, wild-type (WT) and *Eed* cKO mice were immunized to establish the EAE model. As anticipated, *Eed* cKO mice exhibited milder EAE symptoms throughout the disease progression and demonstrated reduced demyelination in the CNS when compared to WT mice (Fig. 6A–C). As expected, we observed a significant decrease in inflammatory infiltration within the CNS of *Eed* cKO EAE mice at dpi 23, as evidenced by the reduced frequencies and total proportion and numbers of $CD4^+IFN\text{-}\gamma^+$ Th1 cells and $CD4^+IL\text{-}17^+$ Th17 cells (Fig. 6D–F), alongside increased differentiation of anti-inflammatory $CD4^+IL\text{-}4^+$ Th2 cells and $CD4^+Foxp3^+$ Treg cells (Fig. 6G, H). Notably, flow cytometry analysis revealed a significant reduction in the percentage and numbers of $CD11c^+MHC\text{-}II^+$ DCs within the CNS of *Eed* cKO EAE mice (Fig. 6I, J). Besides, lower mRNA levels of *Ifn-γ* and increased expression of the anti-inflammatory cytokine *Il-4* were observed in the brain of *Eed* cKO EAE mice, further confirming that *Eed* deficiency in DCs impedes neuroinflammation in EAE model (Fig. 6K).

Furthermore, we also investigated peripheral immune activation in EAE mice. The percentages and total numbers of pro-inflammatory Th1 ($CD4^+IFN\text{-}\gamma^+$) and Th17 ($CD4^+IL\text{-}17^+$) cells in the draining lymph nodes of *Eed* cKO EAE mice were suppressed notably when compared to WT EAE mice, while the differentiation of anti-inflammatory Th2 ($CD4^+IL\text{-}4^+$) and Treg ($CD4^+Foxp3^+$) cells were increased (Fig. 7A–E). Importantly, the proportions and total numbers of $CD11c^+$ DCs and $CD11c^+CD80^+$ mature DCs were markedly lower in the spleen of *Eed* cKO mice, while the ratio of $CD80^+$ mature DCs within the total $CD11c^+$ DC population remained unchanged (Fig. 7F–I). This suggested that DC migration, rather than maturation, was impaired in *Eed* cKO EAE mice. In addition, we also examined the levels of autoimmune responses in the draining lymph nodes during the plateau phase of EAE. Results showed that *Eed* deficiency continued to suppress the proportions and numbers of Th1, Th17 and DCs at dpi 30 (Supplementary Fig. 1). Overall, these data confirmed that mice lacking *Eed* in DCs exhibit resistance to DC migration and EAE development, which is similar to the effects of EED inhibitors.

EED inhibitors suppress human DC migration

In order to substantiate the applicability of EED inhibitors and EED as a target in humans, we conducted experiments to assess its role in modulating the inflammatory responses of human monocyte-derived dendritic cells (moDCs). $CD14^+$ monocytes were isolated using magnetic sorting and induced to differentiate into immature moDCs through exposure to human GM-CSF and IL-4. Subsequently, these cells were treated with EED inhibitors and stimulated with LPS to induce maturation (Fig. 8A). The morphological transitions from $CD14^+$ monocytes (Day 0) to immature moDCs (Day 3), and subsequently to LPS-stimulated mature moDCs (Day 6 and Day 7), were observable under microscopic examination (Fig. 8B). Additionally, the expression of CD209, a marker absent in monocytes but prominently expressed by moDCs, served as a confirmatory indicator of successful moDC differentiation (Fig. 8C).

(See figure on next page.)

Fig. 3 EED inhibitors mediate the transcriptional programs for DC migration. **A** PCA of the transcriptome profiles of DC2.4 after treating with EEDi-5285 (5 μM) for 24 h and LPS (50 ng/mL) for 6 h. $n = 3$ independent experiments. **B** Volcano plot of the transcriptome profiles from vehicle and EEDi-5285 group (fold-change > 2, $P < 0.05$). **C** Heatmap analyses of the differentially expressed genes vehicle and EEDi-5285 group. **D** GSEA analyses of genes enriched in vehicle or EEDi-5285 group. **E** The relative counts of indicated genes in DC2.4 from vehicle and EEDi-5285 group. **F–H** GSEA enrichment scores for indicated gene sets in vehicle or EEDi-5285 group. **I** The relative counts of indicated genes in DC2.4 from vehicle and EEDi-5285 group. Data are presented as mean ± SD. *, $P < 0.05$; **, $P < 0.01$; ***, $P < 0.001$

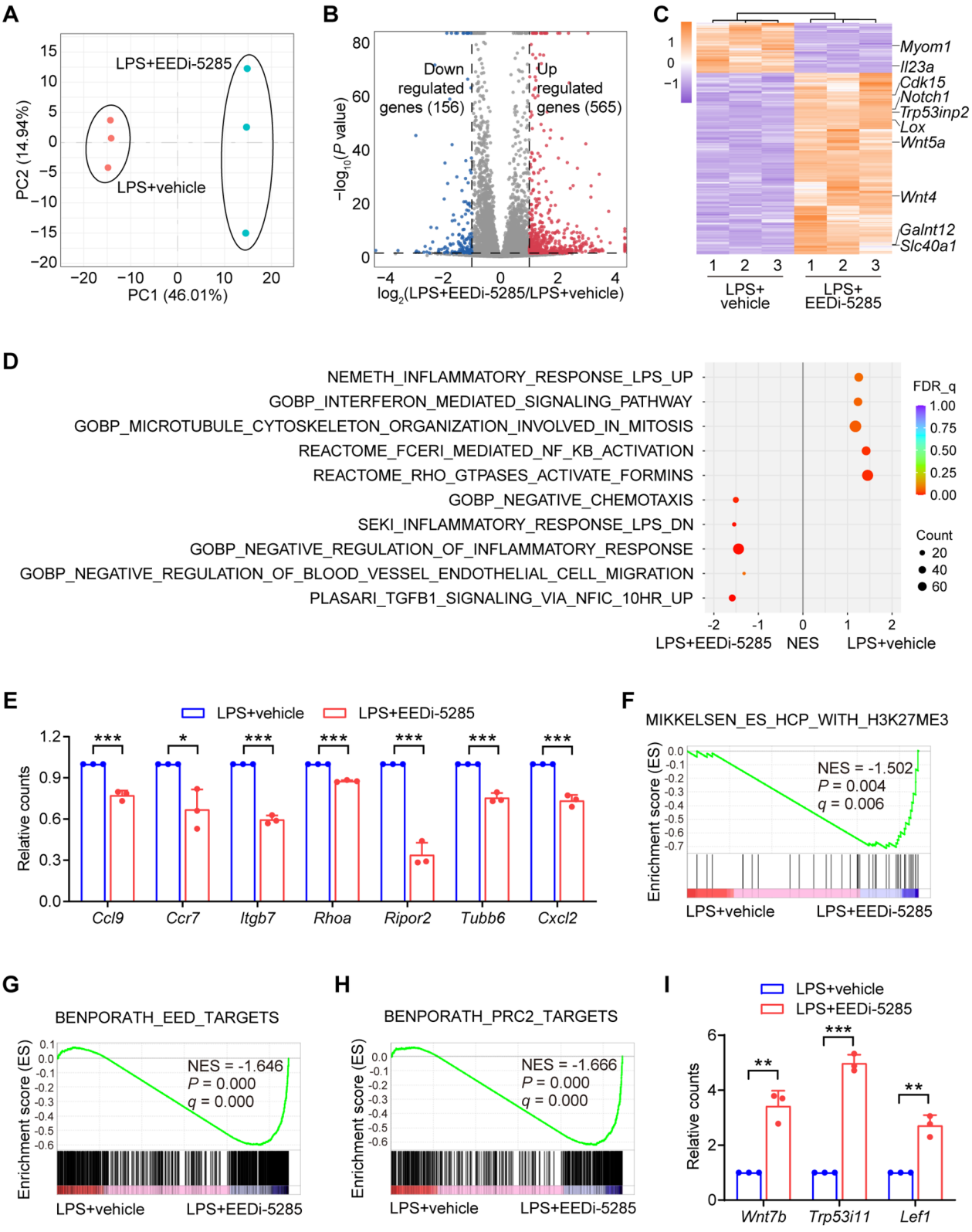

Fig. 3 (See legend on previous page.)

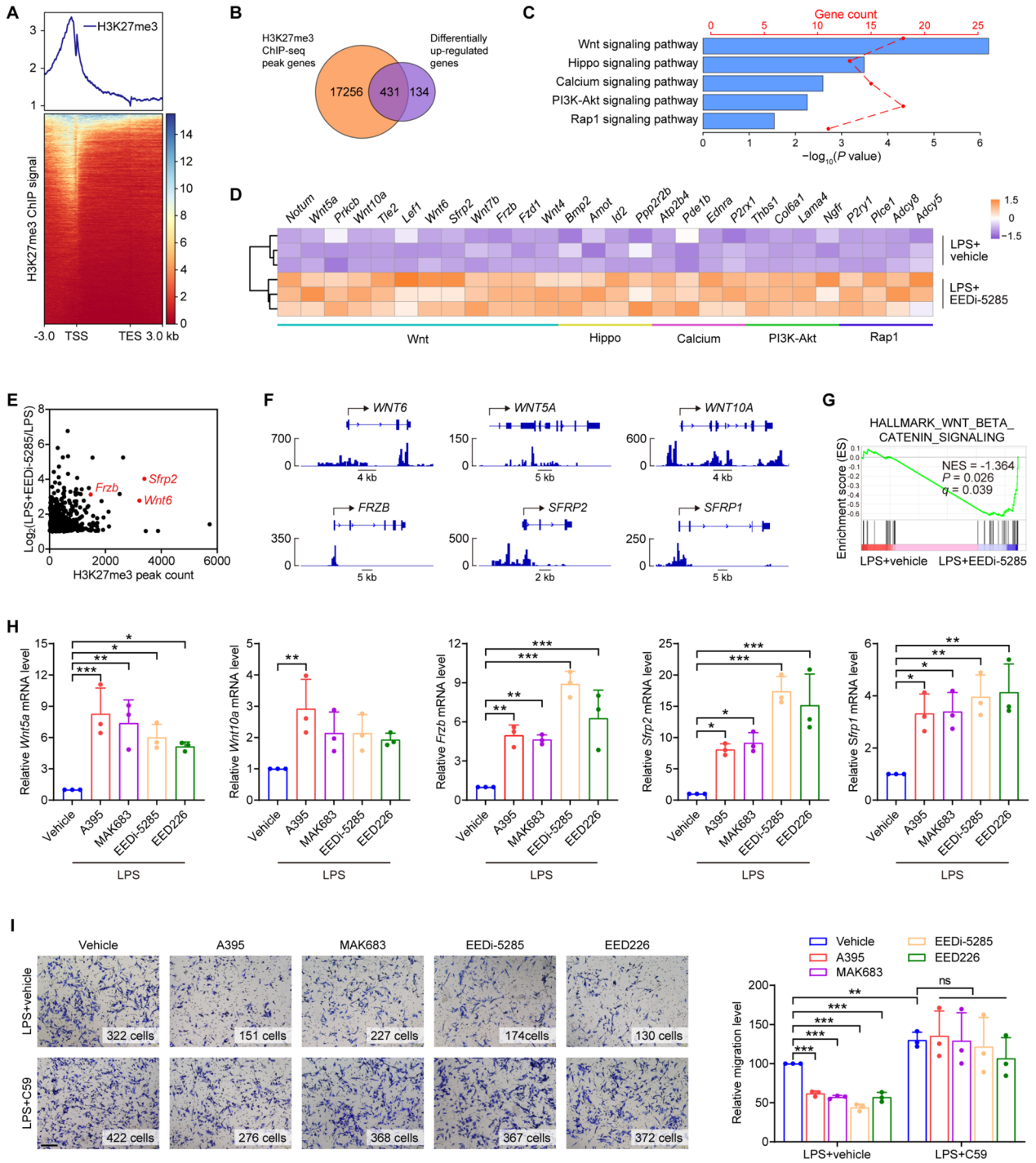

Fig. 4 EED inhibitors block DC migration via promoting WNT signaling. **A** ChIP-seq analyses of H3K27me3 enrichment around TSS and TES regions in human DCs from GEO dataset GSE209566. Genes shown in rows were sorted in decreasing order by signal intensity. **B** Venn diagram of the overlapped genes between the H3K27me3-bound genes in DCs and differentially up-regulated genes in EEDi-5285 group. **C** KEGG analyses of the signaling pathways that enriched in the 431 overlapped genes from (**B**). **D** Heatmap analyses of the representative genes involved in different pathways of (**C**) in vehicle and EEDi-5285 groups. **E** Bland–Altman plot showing H3K27me3 ChIP-seq peaks in DCs with upregulated genes in EEDi-5285 group. **F** Representative H3K27me3 ChIP-seq peak tracks of indicated genes in DCs. **G** GSEA enrichment scores for WNT signaling in EEDi-5285group. **H** qRT-PCR analyses of the mRNA levels of WNT-related genes after treatment with A395 (5 μM), MAK683 (5 μM), EEDi-5285 (5 μM) or EED226 (10 μM) for 24 h and LPS (50 ng/mL) for 6 h. $n = 3$. **I** Representative images (left) and statistics (right) for transwell analysis together with crystal violet staining in DC2.4 after treating with Wnt-C59 (5 μM), A395 (5 μM), MAK683 (5 μM), EEDi-5285 (5 μM) or EED226 (10 μM) for 24 h and LPS (50 ng/mL) for 6 h. Scale bar: 200 μm. $n = 3$. Data are presented as mean ± SD. *, $P < 0.05$; **, $P < 0.01$; ***, $P < 0.001$; ns, not significant

Western blotting analysis suggested that EED inhibitors distinctly suppressed the levels of H3K27 trimethylation in moDCs by specifically targeting the H3K27me3 binding pocket of EED protein (Fig. 8D). In alignment with observations in murine cells, EED inhibitors enhanced the expression of WNT/β-catenin-responsive genes and substantially impaired the chemotactic response of mature moDC migration to CCL19 and CCL21 (Fig. 8E–G). However, the expression of CD83, a co-stimulatory factor for human DC activation, was marginally affected by EED inhibitors, while the levels of MHC-II remained unchanged (Fig. 8H, I). Notably, with the exception of EED226, which decreased the production of TNF-α in moDCs, other EED inhibitors exerted minimal influence on the secretion of pro-inflammatory cytokine TNF-α and anti-inflammatory cytokine IL-10 (Fig. 8J). This suggested a modest role for EED in the maturation of DCs. Taken together, our results highlighted an obstructive role of EED inhibitors in the migration of human DCs, potentially making EED a promising therapeutic target for human autoimmune disorders.

Discussion

Dendritic cells are pivotal in orchestrating both the innate and adaptive immune responses, playing a critical role in maintaining tissue homeostasis and regulating immune-mediated diseases such as MS [21, 33, 34]. Upon activation, DCs capture antigens and subsequently migrate to the meningeal lymphoid vessels in a CCL19/21-mediated manner, thereby initiating CNS inflammation characteristic of MS [35]. In early-phase preclinical trials, the adoptive transfer of tolerogenic immature DCs or strategies aimed at reducing DC migration have shown promise in MS therapy [8, 36]. However, small molecule compounds targeting DCs that are currently under investigation remain either unsuccessful or in the preclinical phase. In this study, we demonstrated that both EED inhibitors and the selective deletion of *Eed* significantly suppressed DC migration and alleviated EAE through activating WNT pathway. Yet four allosteric EED inhibitors are currently in clinical trials for cancer treatment [6, 37], our findings may provide a promising strategy of targeting DC for MS treatment.

Administration of EED266 in vivo mitigated the symptoms of EAE, which may be attributed to the suppression of DC migration (Fig. 1). However, it is important to acknowledge the indispensable roles of PCR2 or H3K27me3 in other immune cells, such as T cells, B cells, and macrophage [17, 38, 39], which are crucial for MS progression. Thus, it is also of interest to investigate the involvement of these other immune cells in the context of EAE in mice treated with EED226. In vitro, we evaluated the effects of various EED allosteric inhibitors on modulating DC phenotypes, and found similar inhibitory effects on global H3K27me3 levels, as well as on migration of DCs at the concentrations used in our study (Fig. 2). Notably, both MAK683 and EEDi-5285 were optimized based on EED226, with EEDi-5285 showing approximately 100 times greater potency in binding to EED [7, 24]. This increased potency may partially account for the higher concentration requirement of EED226. However, further research is needed to elucidate the differential immunomodulatory effects of these four inhibitors on DCs and to assess the in vivo effectiveness of other small molecules beyond EED226.

Indeed, the four EED inhibitors examined in this study are capable of binding to EED within the pocket that recognizes the trimethyl lysine head group of H3K27me3, thereby disrupting the catalytic activity of PRC2 [23]. Homology comparisons indicate that the EED protein sequence is identical in mice and humans, and EZH2 shows a high degree of conservation (98.39% sequence identity), with only two amino acid differences in the EZH2-EED interaction region and a completely conserved SET catalytic domain [25]. This suggests that EED inhibitors might maintain their PRC2 inhibitory function

(See figure on next page.)

Fig. 5 EED deficiency impedes DC activation. **A** Diagram depicting generation of *Eed* cKO mice. **B** Western blotting analysis (left) and its corresponding quantification (right) for the expression of EED and H3K27me3 in WT or *Eed* cKO BMDCs. $n = 3$. **C**, **D** Representative images and bar graph for flow cytometry analysis of the percentage and number of $CD11c^+$ cells in WT or *Eed* cKO BMDCs after treating with LPS (50 ng/mL) for 6 h. $n = 3$. **E**, **F** Representative images (**E**) and bar graph (**F**) for flow cytometry analysis of the percentages and numbers of $CD80^+$, $CD86^+$ or MHC-II^+ cells in $CD11c^+$ DCs of WT or *Eed* cKO BMDCs after treatment of LPS (50 ng/mL) for 6 h. $n = 3$. **G** Representative images (left) and quantification (right) for transwell analysis of chemokines-triggered migration of WT or *Eed* cKO BMDCs after treating with EEDi-5285 (5 μM) or EED226 (10 μM) for 24 h and LPS (50 ng/mL) for 6 h. $n = 5$. **H** Representative images (left) and bar graph (right) for flow cytometry analysis of the frequency of Th1 ($CD4^+$IFN-γ^+) and Th17 ($CD4^+$IL-17^+) cells after co-culture with MOG_{35-55} (30 μg/mL, 24 h) and LPS (50 ng/mL, 6 h) stimulated WT or *Eed* cKO BMDCs. $n = 3$. **I** qRT-PCR analyses of the indicated WNT genes in WT or *Eed* cKO BMDCs after treatment with LPS (50 ng/mL) for 6 h. $n = 3$. **J** CUT&Tag-qPCR analyses of the enrichment of H3K27me3 in the promoters of WNT genes in WT or *Eed* cKO BMDCs after treatment with LPS (50 ng/mL) for 6 h. $n = 3$. **K** Quantification for transwell analysis of chemokines-triggered migration of WT or *Eed* cKO BMDCs after treating with Wnt-C59 (5 μM) for 24 h and LPS (50 ng/mL) for 6 h. $n = 6$. Data are presented as mean ± SD. *, $P < 0.05$; **, $P < 0.01$; ***, $P < 0.001$; ns, not significant

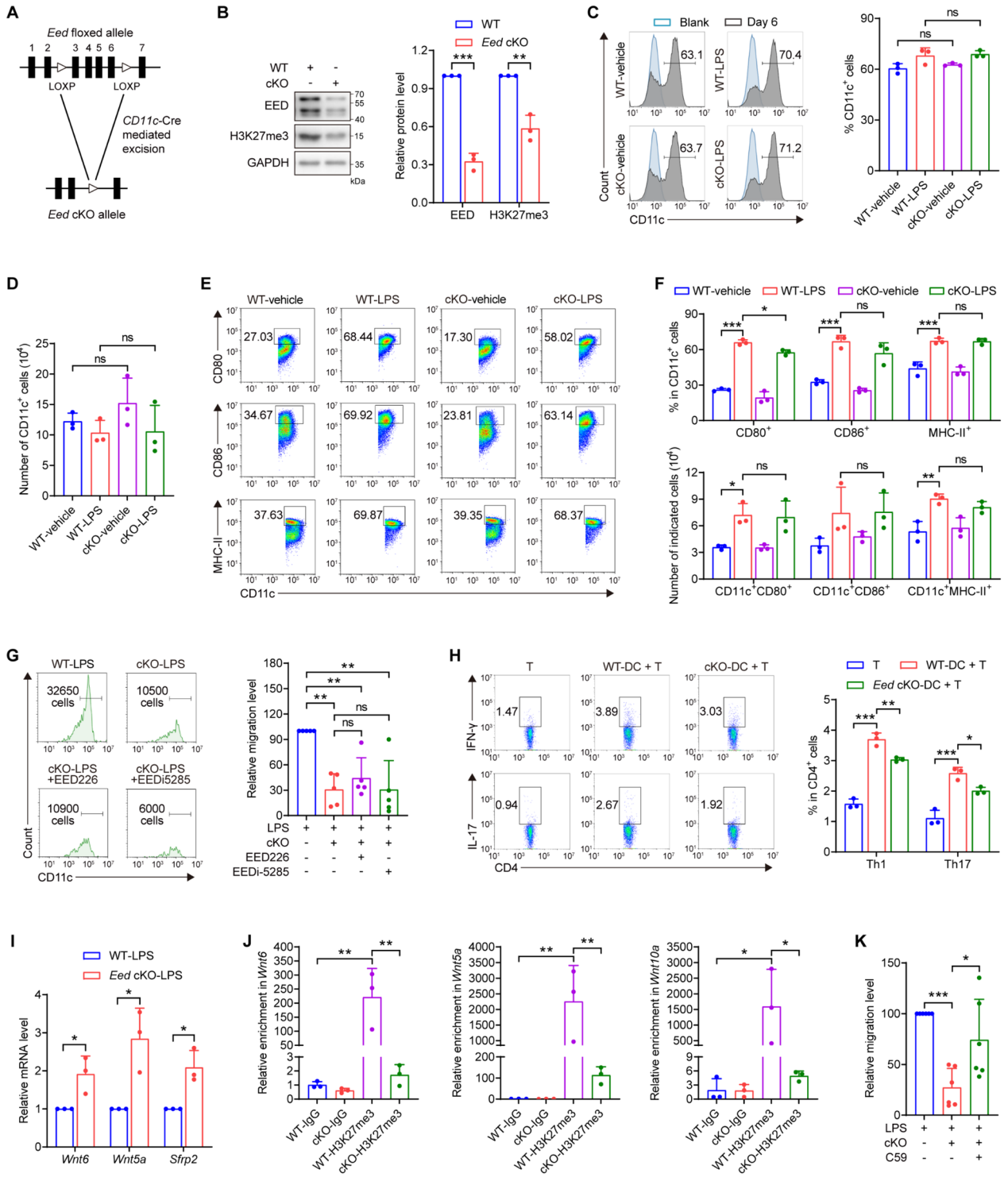

Fig. 5 (See legend on previous page.)

in mice and humans. As expected, these four EED inhibitors also suppressed inflammatory activation in human moDCs (Fig. 8), hinting at their potential clinical efficacy. Given the potential impact of minor PRC2 protein sequence variations on allosteric mechanisms, further research is warranted to understand the role of EED inhibitors in human diseases. This should be done using humanized EAE animal models to provide more insight

into their therapeutic potential. Although network-based analysis in cerebrospinal fluid has identified *Eed* as a potential candidate gene for MS therapy [11], further studies are required to elucidate the clinical relevance of EED to MS.

Extensive alterations of H3K27me3 modification have been observed following LPS stimulation in DCs [40]. Zbtb46, HSP70L1, and miR-155 are known to regulate DC maturation and migration by mediating H3K27me3 deposition at the *Cd80*, *Cd86*, and *Ccr7* genes, respectively [18, 19, 41]. In addition, *Suz12* ablation disrupts the maintenance of H3K27me3 mark, resulting in a swift depletion of tissue-resident dendritic cells, including Langerhans cells, under both steady-state and inflammatory conditions because these cells could no longer proliferate to facilitate their self-renewal [15]. While the impact of reduced H3K27me3 levels due to *Suz12* depletion on DC migration remains to be elucidated, these findings underscore the potential role of H3K27me3 in modulating DC functions.

The Jumonji domain-containing protein 3 (JMJD3) is a pivotal demethylase responsible for H3K27me3 removal, thereby facilitating gene expression. Typically, JMJD3 and PRC2 have opposing roles, with H3K27me3 representing a dynamic equilibrium between the activities of methyltransferases and demethylases. However, genetic depletion of *Jmjd3* in $CD4^+$ T cells has been shown to impede EAE progression by enhancing H3K27me3 levels at the *Rorc* locus, which is associated with pro-inflammatory Th17 cells [42]. The JMJD3 inhibitor GSK-J4 is found to promote an immune tolerance phenotype in DCs and to mitigate EAE-associated inflammation, potentially through modulating the balance of H3K27me3 and H3K4me3 modifications [43]. Additionally, GSK-J4 administration ameliorates symptoms in inflammatory bowel disease and rheumatoid arthritis by regulating H3K27me3 binding at the promoters of various inflammatory genes [44–47]. Some researchers propose that JMJD3 is selectively recruited to transcription start sites with high H3K4me3 levels, as the overall H3K27me3 levels are not significantly affected by the absence of *Jmjd3*, highlighting a H3K27me3-independent role of JMJD3 [48]. Interestingly, our preliminary data suggest that GSK-J4 may also hinder DC migration (Supplementary Fig. 2), an effect that mirrors the impact of EED inhibitors. It is essential to continue investigating the diverse functions of various epigenetic regulators related H3K27me3.

In addition to modulating histone methylation, a growing amount of research indicates that EED, along with other PRC2 components, exerts significant effects on various biological processes in a manner that is independent of their epigenetic functions. For instance, in *Eed*-inactivated cardiomyocytes, gene upregulation was not associated with a reduction in H3K27me3 levels. Instead, EED was found to interact with histone deacetylases, modulating the catalytic activity of H3K27ac, which is crucial for the development of cardiomyocytes and the maintenance of normal cardiac function [49]. Similarly, the knockout of *Ezh2*, another PRC2 subunit, didn't alter H3K27me3 levels in DCs, but regulated DC adhesion dynamics and extranuclear integrin signaling, thereby ameliorating EAE [14, 15]. It is noteworthy that our study identified EED inhibitors markedly reduced H3K27me3 levels, and targeting the downstream genes regulated by H3K27me3 counteracted the pharmaceutical effects of EED inhibitors on DCs (Figs. 3, 4). This suggests that H3K27me3 is likely to be involved in the observed effects. However, further research is warranted to explore the non-epigenetic functions of EED and to elucidate the full spectrum of its biological roles.

In our study, we demonstrated that the inhibition of EED suppresses DC migration by enhancing WNT signaling (Figs. 4, 5). This finding is in line with existing research, which has established that the WNT/β-catenin signaling pathway is essential for maintaining the immunological tolerance of DCs in intestinal and CNS inflammation. This signaling cascade is believed to modulate its effects by regulating the expression of retinoic acid-metabolizing enzymes, IL-10, and TGF-β

(See figure on next page.)

Fig. 6 *Eed* deficiency in DC suppresses EAE progression. **A** Clinical score in WT and *Eed* cKO EAE mice. $n = 14$ animals, 9 animals are sacrificed for the histopathological examination and flow cytometry analysis at day 23 post immunization (dpi 23). * indicates a statistically difference when compared with WT group. **B** Representative images (left) and bar graph (right) of LFB staining for spinal cords from WT and *Eed* cKO EAE mice at dpi 23. Scale bar: 50 μm. $n = 3$. **C** Representative images (left) and bar graph (right) for electron microscopy analysis of the demyelination in the spinal cords from WT and *Eed* cKO EAE mice at dpi 23. Scale bar: 2 μm. $n = 3$. **D**–**F** Representative images (D) and bar graph (E, F) for flow cytometry analysis of the percentages and numbers of Th1 ($CD4^+IFN\text{-}\gamma^+$) and Th17 ($CD4^+IL\text{-}17^+$) in the brains from WT and *Eed* cKO EAE mice at dpi 23. $n = 3$. **G** Immunostaining of CD4 (green) and IL-4 (red) in the spinal cords from WT and *Eed* cKO EAE mice at dpi 23. Scale bar: 50 μm. $n = 3$. **H** Immunostaining of CD4 (red) and Foxp3 (green) in the spinal cords from WT and *Eed* cKO EAE mice at dpi 23. Scale bar: 50 μm. $n = 3$. **I**, **J** Representative images (**I**) and bar graph (**J**) for flow cytometry analysis of the frequency and numbers of $CD11c^+MHC\text{-}II^+$ DCs in the brains from WT and *Eed* cKO EAE mice at dpi 23. $n = 3$. **K** qRT-PCR analyses for the mRNA levels of pro-inflammatory cytokines *Ifn-γ* and anti-inflammatory cytokine *Il-4* in the brains from WT and *Eed* cKO EAE mice at dpi 23. $n = 3$. Data are presented as mean ± SD. *, $P < 0.05$; **, $P < 0.01$; ***, $P < 0.001$

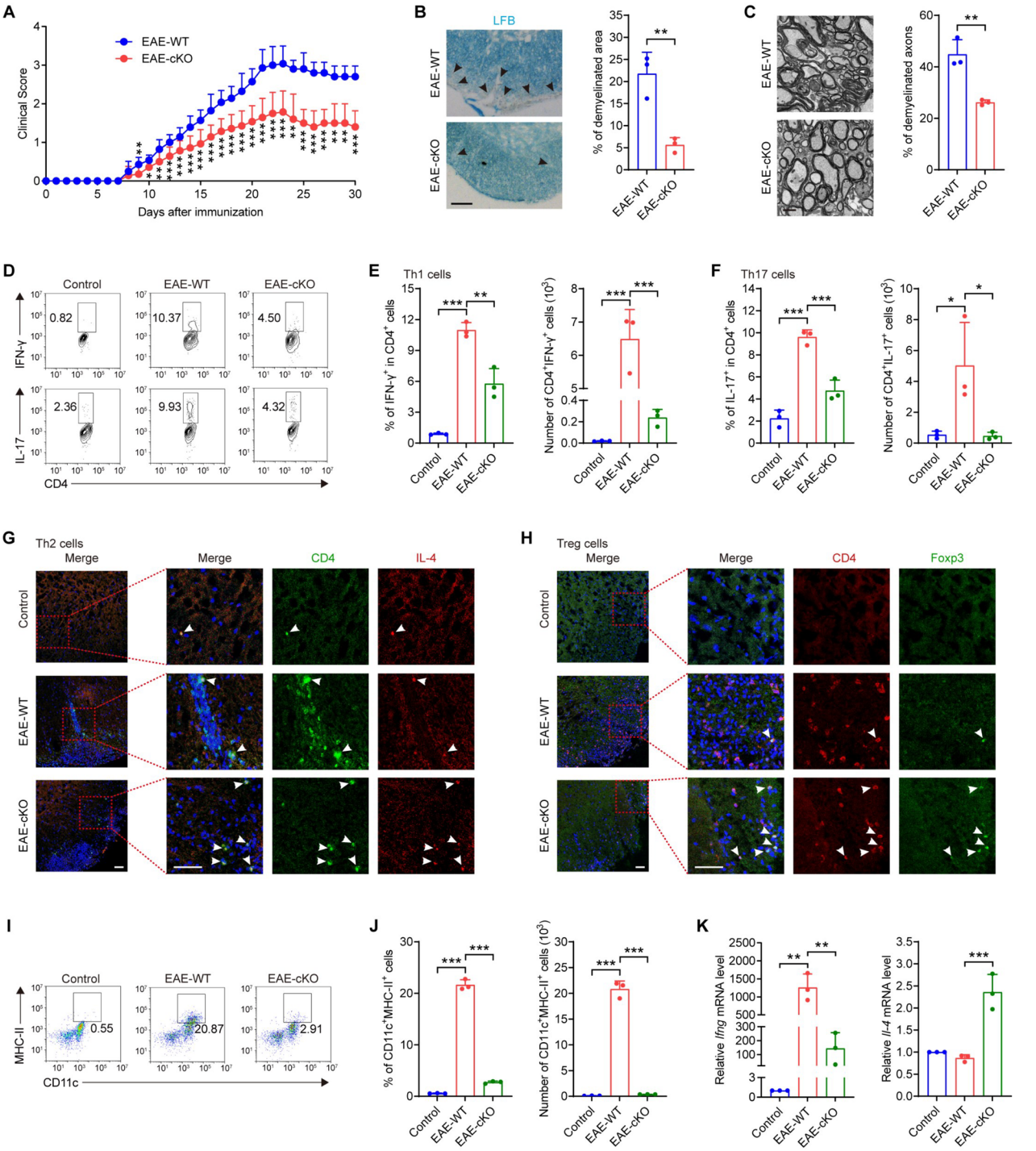

Fig. 6 (See legend on previous page.)

[50, 51]. Similarly, WNT-1 overexpression in the lung resulted in reduced migration of allergen-loaded DCs from the lung to the draining lymph nodes [52]. Besides, a study observed reduced expression of β-catenin and an increased propensity for migration to skin-draining lymph nodes in *Raptor*-deficient Langerhans cells (skin DCs), highlighting the importance of the WNT/β-catenin pathway in DC migration [53]. Interestingly, WNT has also been identified as a significant target for epigenetic modification by EED in a variety of cell types, including

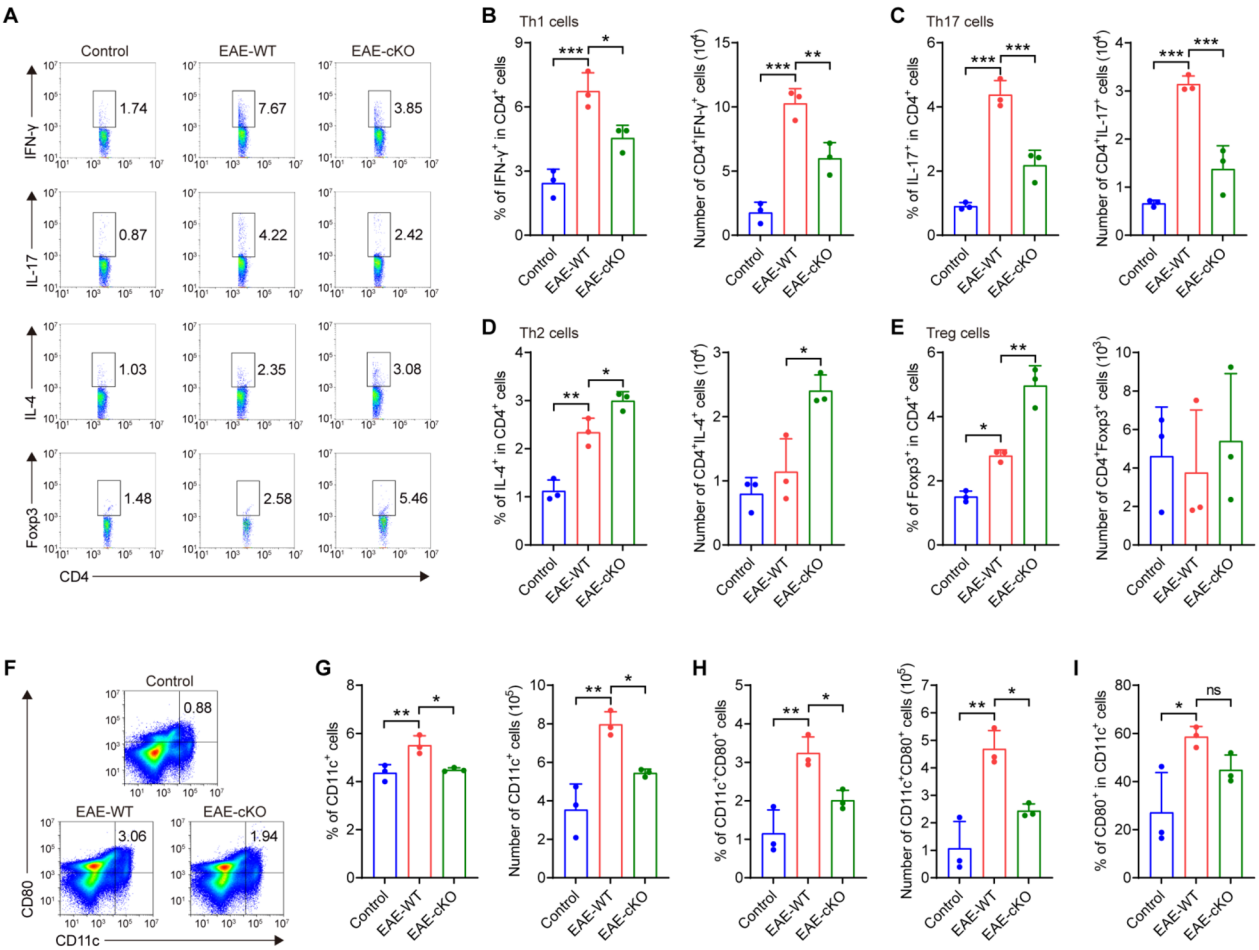

Fig. 7 *Eed* loss alleviates periphery inflammation in EAE mice. **A**–**E** Representative images (**A**) and bar graph (**B**–**E**) for flow cytometry analysis of the percentages and numbers of Th1 ($CD4^+IFN\text{-}\gamma^+$), Th17 ($CD4^+IL\text{-}17^+$), Th2 ($CD4^+IL\text{-}4^+$) and Treg ($CD4^+Foxp3^+$) in the draining lymph nodes from WT and *Eed* cKO EAE mice at dpi 23. $n = 3$. **F–H** Representative images (**F**) and bar graph (**G**, **H**) for flow cytometry analysis of the percentages and numbers of total DCs ($CD11c^+$) and mature DCs ($CD11c^+CD80^+$) in the spleen from WT and *Eed* cKO EAE mice at dpi 23. $n = 3$. **I** Bar graph for flow cytometry analysis of the percentage of $CD80^+$ in $CD11c^+$ DCs in the spleen from WT and *Eed* cKO EAE mice at dpi 23. $n = 3$. Data are presented as mean ± SD. *, $P < 0.05$; **, $P < 0.01$; ***, $P < 0.001$; ns, not significant

(See figure on next page.)

Fig. 8 EED inhibitors hinder the chemotaxis of human moDCs. **A** Scheme of human moDCs culture and inflammation-associated phenotype detection. **B** The morphological changes from monocytes (Day0) to immature moDCs (Day 6) and eventually LPS-challenged mature moDCs (Day7). Scale bar: 20 μm. $n = 3$. **C** Representative images (left) and bar graph (right) for flow cytometry analysis of the frequency of $CD209^+$ moDCs after cell culture for 7 days. $n = 3$. **D** Western blotting analysis (left) and its corresponding quantification (right) for the expression of EED and H3K27me3 in human moDCs treated with A395 (5 μM), MAK683 (5 μM), EEDi-5285 (5 μM), EED226 (10 μM) and LPS (300 ng/mL) for 24 h. $n = 3$. **E** qRT-PCR analyses of the mRNA levels of WNT-related genes in human moDCs treated with EEDi-5285 (5 μM), EED226 (10 μM) and LPS (300 ng/mL) for 24 h. $n = 3$. **F**, **G** Representative images (**E**) and statistics (**F**) for transwell analysis in human moDCs after treating with A395 (5 μM), MAK683 (5 μM), EEDi-5285 (5 μM), EED226 (10 μM) and LPS (300 ng/mL) for 24 h. Scale bar: 200 μm. $n = 3$. **H**, **I** Representative images (**H**) and bar graph (**I**) for flow cytometry analysis of the expression of CD83 and HLA-DR (MHCII) in $CD209^+$ moDCs after treatment with A395 (5 μM), MAK683 (5 μM), EEDi-5285 (5 μM), EED226 (10 μM) and LPS (300 ng/mL) for 24 h. $n = 3$. **J** Elisa of TNF-α and IL-10 levels in the supernatant of human moDCs after treatment with A395 (5 μM), MAK683 (5 μM), EEDi-5285 (5 μM), EED226 (10 μM) and LPS (300 ng/mL) for 24 h. $n = 3$. Data are presented as mean ± SD. *, $P < 0.05$; **, $P < 0.01$; ***, $P < 0.001$

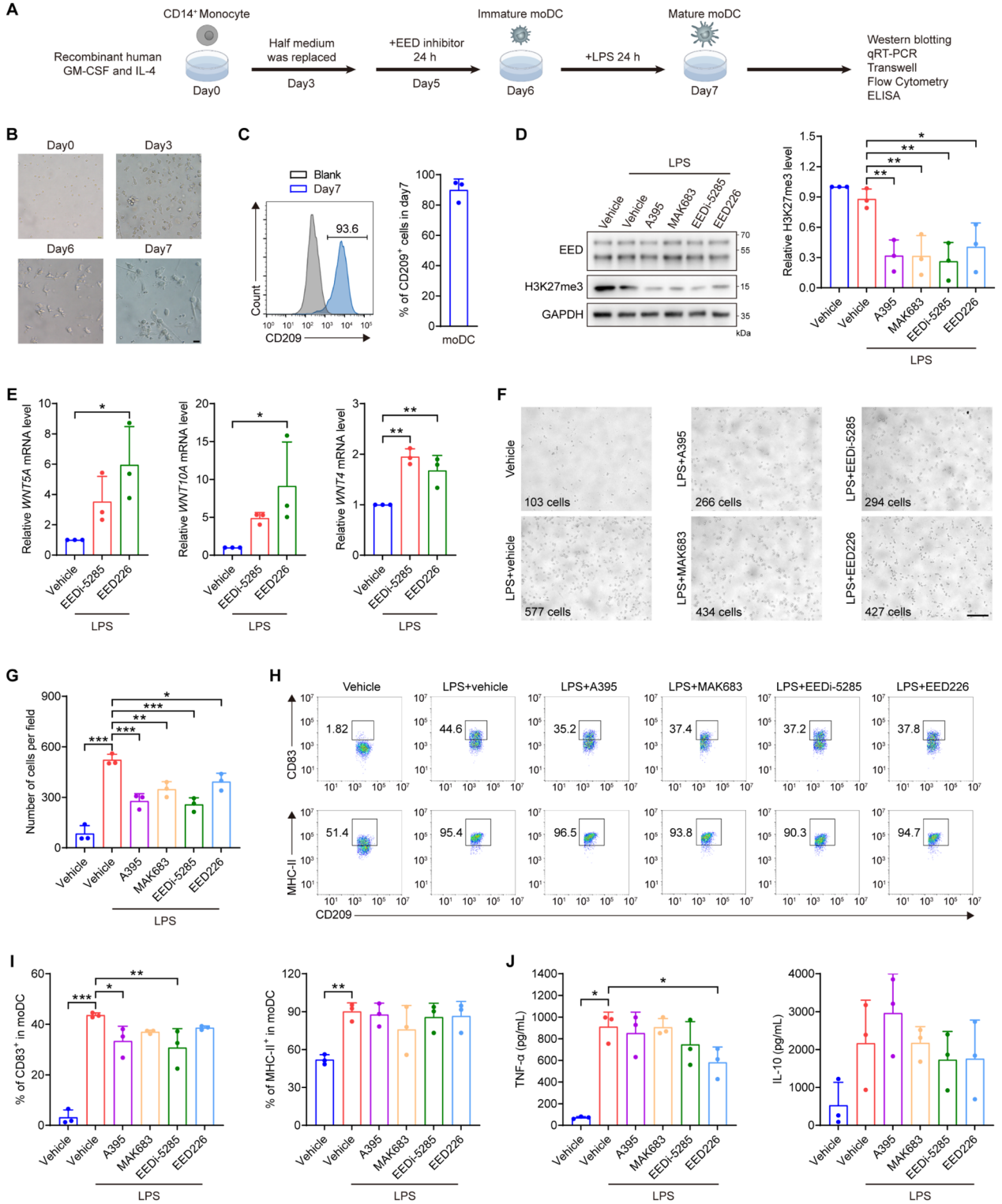

Fig. 8 (See legend on previous page.)

intestinal stem cells, chondrocytes, and oligodendrocytes [4, 54, 55]. Despite these insights, it remains to be determined whether in vivo modulation of WNT signaling can reverse the ameliorative effects of EED deficiency in EAE. Additionally, the potential involvement of other mechanisms in the DC inactivation mediated by EED inhibitors warrants further investigation.

In summary, our study introduces a potential novel therapeutic application of EED inhibitors in mitigating CNS inflammation through the inactivation of DCs. We have demonstrated that H3K27me3-dependent WNT signaling is essential for the immunomodulatory effects of EED inhibitors. By targeting DC activation and modulating epigenetic modifications, our research not only proposes a novel strategy for autoimmune disease treatment but also underscores the pivotal role of EED in maintaining DC homeostasis. This insight may pave the way for DC-based therapies in the management of autoimmune diseases, offering a promising avenue for future research and clinical development.

Materials and methods

Mice

Eed$^{flox/flox}$ mice were gifted by Prof. Q. Richard Lu [4], and *CD11c*-Cre mice were obtained from the Jackson Laboratory [21]. The CD11c^{+} cells conditional *Eed* knockout (*Eed* cKO) mice were generated by breeding *CD11c*-Cre with *Eed*$^{flox/flox}$ transgenic mice. All mice were fed in a specific pathogen-free environment with 60 ± 5% humidity, 21 ± 1 °C, and 12 h light/dark cycle, and provided with standard laboratory diet and water ad libitum. All animal studies were performed in compliance with all relevant ethical regulations and approved by the Institutional Animal Care and Use Committee (IACUC) at Zhejiang University (IACUC-s21-017).

Induction and assessment of EAE

EAE mouse model was induced as described previously [21, 56]. In brief, 8-week-old C57BL/6 female mice were immunized with 400 μg MOG_{35-55} peptide (Sangom Biotech) emulsified 1:1 in CFA (Sigma, F5881) containing 5 mg/mL heat-killed Mycobacterium tuberculosis H37Ra (BD Difco, 231141) subcutaneously at day 0. Besides, 100 μL PBS containing 200 ng pertussis toxin (List Biological Laboratories, #181) was administered intravenously at day 0 and day 2 post-immunization per mouse.

All mice were subsequently monitored for the signs of EAE daily and finally sacrificed at day 22–23 or day 30 for evaluation. Every animal will receive a clinical score from 0 to 4 as follows: 0, healthy; 0.5, limp of tail tip; 1, complete tail limp; 1.5, powerless of one hindlimb; 2, powerless of tow hindlimb; 2.5 paralysis of one hindlimb; 3, complete hindlimb paralysis; 3.5, paralysis of forelimb; 4, severe paralysis or death [21, 56].

Histological staining

For hematoxylin and eosin (H&E) staining, spinal cords collected from paraformaldehyde (PFA) perfused EAE mice were fixed in 10% formalin for at least 2 days followed by paraffin embedding. Then 3-μm thick sections were deparaffinized and stained with H&E. For luxol fast blue (LFB) staining, spinal cords collected from PFA perfused EAE mice were fixed in 4% PFA for 2 h followed by dehydration in 25% saccharose for 14 h and embedded in OCT (SAKURA Finetek, 4583). Then 12-μm thick sections were stained with LFB (Sigma-Aldrich, S3382) overnight, rinsed in distilled water, differentiated with 0.05% lithium carbonate and 70% ethanol, and finally stopped by distilled water.

Electron microscopy

For electron microscopy analysis, fresh spinal cord tissues were fixed in 2.5% glutaraldehyde for a minimum of 2 days, followed by postfixation in 1% OsO_4 for 1.5 h. Subsequently, the tissues were stained with uranyl acetate and lead citrate, and then cut into ultrathin sections. The sections were finally examined using a Spirit 100 kV electron microscope (PHILIPS TECNAI 10).

Cell culture

DC2.4 cell line was cultured in RPMI-1640 containing 10% fetal bovine serum, 100 mg/mL streptomycin, and 100 mg/mL penicillin. Cells were maintained in a humidified atmosphere containing 5% CO2 at 37 °C.

For BMDC isolation and culture, bone marrow from 6 to 8 week old C57BL/6 mice were resuspended and cultured in RPMI-1640 medium supplemented with 10% fetal bovine serum, 100 mg/mL streptomycin, 100 mg/mL penicillin, 20 ng/mL recombinant murine IL-4 (Peprotech, 214-14), and 50 ng/mL recombinant murine GM-CSF (Peprotech, 315-03). Half medium supplemented with cytokines was replaced by fresh medium at day 3, and used at day 6 as immature BMDCs.

For human monocyte-derived dendritic cells (moDCs) culture, monocytes were purified from peripheral blood mononuclear cells using anti-CD14 microbeads (Miltenyi, 130–050-201) and cultured into moDCs in RPMI-1640 medium supplemented with 10% fetal bovine serum, 100 mg/mL streptomycin, 100 mg/mL penicillin, 100 ng/mL recombinant human IL-4 (Peprotech, 200–04) and 100 ng/mL recombinant human GM-CSF (Peprotech, 300–03). Half medium was replaced by fresh medium at day 3 and day 5, and used at day 6 as immature moDCs. Human blood sample collection was in accordance with the Ethical Review Consent Letter

approved by Beijing Boren Hospital Ethics Committee (No. 20211126-TY-001 K).

Chemical treatment

In EAE mouse model, EED226 (40 mg/kg, dissolved in 5% DMSO + 95% saline solution) or solvent control was given by i.g. twice a day from day 7.

For DC activation, cells were treated with 50 ng/mL LPS (Aladdin, L118716) for 6 h in DC2.4 or BMDCs, 300 ng/mL LPS for 24 h in moDCs. For compounds intervention (except cell viability assay), cells were treated with 5 μM A395 (TargetMol, T10205) for 24 h, 5 μM MAK683 (TargetMol, T15201) for 24 h, 5 μM EEDi-5285 (TargetMol, T22322) for 24 h, 10 μM EED226 for 24 h, or 5 μM Wnt-C59 (TargetMol, T2242) for 24 h.

Cell viability assay

DC2.4 were seeded into 96-well plates at 6000 cells/well for 24 h, and different concentrations of A395, MAK683, EEDi-5285 or EED226 (0, 0.32, 0.63, 1.25, 2.5, 5, 10, 20 and 40 μM) were incubated with DC2.4 for another 24 h.

Sulforhodamine B (SRB) staining was then performed to examine the cell viability. In brief, cells were incubated with 4 mg/mL SRB for 30 min, washed with 1% acetic acid more than 5 times, dissolved with 10 mM Tris-base, and finally detected in 540 nm.

In vitro transwell assay for DC Migration

The transwell assay was performed by 24-well plates together with 8-μm pore size transparent PET membrane (Falcon, 353097). 600 μL culture medium with 100 ng/mL recombinant mouse CCL19 (PeproTech, 250-27B) and CCL21 (PeproTech, 250–13) or 100 ng/mL recombinant human CCL19 (Biolegend, 582102) and CCL21 (Biolegend, 582202) was added to the lower chamber for the migration of BMDCs and DC2.4 or human moDCs, respectively. BMDCs, DC2.4 or moDCs (1×10 [5] cells in a total volume of 200 μL culture medium) were added to the upper chamber. The number of BMDCs or moDCs that migrated to the lower chamber was determined by flow cytometry or microphotography after 4 h, while the number of migrated DC2.4 was visualized by crystal violet staining and microphotography.

Flow cytometry

For cell surface staining, single cell suspensions were incubated with PE anti-mouse CD11c (BioLegend, 117308), FITC anti-mouse CD80 (BioLegend, 104706), PE/Cyanine7 anti-mouse CD86 (BioLegend, 105014), PerCP/Cyanine5.5 anti-mouse MHC-II (BioLegend, 107626), FITC anti-mouse CD4 (BD Biosciences, 553047), PerCP/Cyanine5.5 anti-mouse/human CD44 (BioLegend, 103032), PE anti-mouse CD62L (BioLegend, 104407), PE anti-human CD209 (Biolegend, 330106), APC anti-human CD83 (Biolegend, 305312), or FITC anti-human MHC-II (Biolegend, 327006) for 30 min. Samples were then washed and analyzed by FACS versus flow cytometry (ACEA NovoCyte or BD Biosciences).

For intracellular cytokines staining, lymph glands or central nervous system single cell suspensions were stained with FITC anti-mouse CD4 (BD Biosciences, 553047) for 30 min, followed by staining with PE anti-mouse IFN-γ (BD Biosciences, 554412), PE anti-mouse IL-17A (Biolegend, 506904) or PE anti-mouse IL-4 (eBioscience, 12-7041-82) for 30 min using Cytofix/Cytoperm kit (eBioscience, 00-8222-49) according to the manufacturer's instructions. Intranuclear staining with PE anti-mouse Foxp3 (Biolegend, 126404) was performed using a Fixation/Permeabilization kit (eBioscience, 00-5523-00) according to the manufacturer's protocol.

Elisa for TNF-α and IL-10

The levels of IL-10 and TNF-α in human moDCs supernatant were measured by ELISA (Dakewe, 1111002; Multi Sciences, EK182) according to the manufacturer's protocols. In brief, the supernatant was diluted in a certain proportion and incubated in the coated ELISA plate, followed by biotinylated antibody solution and streptavidin-HRP solution incubation. Finally, ELISA plate is colored by TMB solution and detected in 450 nm.

Co-culture of BMDCs and $CD4^+$ T cells

BMDCs from WT and *Eed* cKO mice were cultured until day 6, and stimulated with 10 μg/mL MOG_{35-55} peptide (Sangom Biotech) for 24 h and 50 ng/mL LPS (Aladdin, L118716) for 6 h. $CD4^+$ T cells were isolated from the spleens and lymph nodes using the MojoSort™ Mouse CD4 T Cell Isolation Kit (Biolegend, 480033), following the manufacturer's protocols. Subsequently, BMDCs and $CD4^+$ T cells were co-cultured at a ratio of 1:10. After 3 days, cells were harvested for the analysis of the percentage of IFN-γ or IL-17A in $CD4^+$ cells by flow cytometry.

Plasmid transfection

Transient transfection was performed using jet medium and jetPRIME (Polyplus, 114–15), according to the manufacturer's instructions, in 12-well plates with 0.5 μg of total DNA per transfection. HA-EED plasmid was constructed by Miaoling Biology.

Western blotting

Cells were washed with PBS and then lysed in the lysis buffer (0.3% NP-40, 0.2% Triton X-100, 0.25% Leupeptin, 0.1% $NaVO_3$, and 0.1% PMSF). Protein extracts were separated by 10% SDS-PAGE and blotted to PVDF

membranes. After blocking with 5% fat-free milk for 1 h at room temperature, strips were incubated with the following primary antibodies overnight at 4 °C: anti-HA (Cell Signaling Technology, #3724), anti-EED (Cell Signaling Technology, #85322), anti-H3K27me3 (Cell Signaling Technology, #9733), anti-GAPDH (Diag-Bio Technology, db106). The strips were further stained by secondary horseradish peroxidase-conjugated IgG for 1 h at room temperature and visualized with enhanced chemiluminescent reagents (NCM Biotech, P2100). Images were finally taken by GE AI100 or Azure biosystem.

Total RNA isolation and quantitative real-time PCR assays

For expression analyses, total RNA extraction was performed using the Trizol reagent (Takara, 9109), and subsequently cDNA reverse transcribed using TransScript kit (TransGen Biotech, AT311-03) according to the manufacturer's protocols. Quantitative real-time RT-PCR reactions were carried out with Taq Pro Universal SYBR qPCR Master Mix (Vazyme, Q712-02), following the reagent manufacturer's specified preset procedure on QuantStudio 6 Flex Real-Time PCR System (Applied Biosystems, Carlsbad, California, USA). The gene expression was normalized to internal control *Gapdh* and determined by the $2^{-\Delta\Delta CT}$ method. PCR primer sequences are available in Supplementary Table 1.

Cleavage under targets and tagmentation—quantitative real-time PCR assays

The CUT&Tag assay was performed using the Novo-NGS® CUT&Tag® 4.0 High-Sensitivity Kit (N259-YH01, NovoProtein, Shanghai, China). Briefly, 1.5×10^5 BMDCs were sequentially incubated with ConA beads for 10 min, anti-H3K27me3 primary antibody (Cell Signaling Technology, #9733) for 2 h, Goat Anti-Rabbit IgG H&L secondary antibody for 1.5 h, and pAG-Tn5 transposase for 1.5 h at room temperature. Subsequently, $MgCl_2$ was added to activate the tagmentation reaction for 1 h at 37 ℃. The transposed DNA fragments were then purified and amplified according to the manufacturer's instructions. The libraries were quantified using quantitative real-time PCR assays and the primer sequences for CUT&Tag-qPCR are provided in Supplementary Table 2.

Immunofluorescence

DC2.4 cells were fixed with 4% PFA at 4 °C for 20 min, permeabilizated by 0.3% Triton X-100 at room temperature for 5 min, and incubated with blocking buffer at room temperature for 15 min. Cells were then stained with Actin-Tracker Green-488 (Beyotime, C2201S) and DAPI (Dojindo, D212) for 45 min at room temperature. For tissue staining, spinal cords collected from PFA perfused EAE mice were fixed in 4% PFA for 2 h followed by dehydration in 25% saccharose for 14 h and embedded in OCT (SAKURA Finetek, 4583). 12-μm thick sections were stained with FITC anti-mouse CD4 (BioLegend, 100406), PE anti-mouse IL-4 (eBioscience, 12–7041-82), PE anti-mouse CD4 (BioLegend, 100408), or anti-FoxP3 (Cell Signaling Technology, #12653) overnight, and then stained with Goat anti-Rabbit IgG (H + L) Cross-Adsorbed Secondary Antibody (Invitrogen, F2765) and DAPI (Dojindo, D212) for 45 min at room temperature. Images were captured by Leica SP8 confocal.

RNA sequencing and data analysis

Total RNA was isolated from LPS + vehicle or LPS + EEDi-5285 treated DC2.4 by Trizol reagent, and subjected to cDNA library construction and RNA sequencing (Novogene). Index of the reference genome was built using Hisat2 (version 2.0.5) and paired-end clean reads were aligned to the reference genome (mm10). Then, featureCounts (version 1.5.0-p3) was used to count the reads numbers mapped to each gene. And the R package DESeq2 (version 1.42.0) was used to identify the differentially expressed genes between the groups ($P < 0.05$ and fold change > 2) for the subsequent analyses.

Raw read counts were first normalized using the DESeq2 variance-stabilizing transformation method to adjust for differences in library size and RNA composition. These normalized counts were then used as input for Gene Set Enrichment Analysis by GSEA software (version 4.3.2). The volcano plot was generated according to https://www.omicstudio.cn/tool. Heatmap was plotted using the R language (version 4.3.1). Kyoto Encyclopedia of Genes and Genomes analysis was performed using DAVID (https://david.ncifcrf.gov/).

ChIP-sequencing analysis

We re-analyzed the published H3K27me3 ChIP-seq data in human DCs from GEO dataset (GSE209566). We utilized bigWigToWig (version 369) to convert the bigWig files into wig format, followed by the transformation of the wig files into BED format using wig2bed (version 2.4.40). Peak calling was performed using MACS2 (version 2.2.7.1). For the visualization of ChIP-seq data, the input bigWig files were processed with deepTools (version 3.5.1). And the bigwig file was imported into IGV software (version 2.8.13) for the analysis of the bindings between H3K27me3 and indicated genes.

Statistical analysis

Statistical comparisons were performed using GraphPad Prism (version 9.5.1). Unpaired two-tailed Student's t-test or one-way ANOVA Tukey's post hoc analysis was used for the comparison between two groups or multiple

comparisons, respectively. All data were presented as means ± SD ($n \geq 3$ independent experiments). The statistical significance was considered when $P < 0.05$ (represented as * $P < 0.05$, ** $P < 0.01$, *** $P < 0.001$).

Supplementary Information

The online version contains supplementary material available at https://doi.org/10.1186/s12974-025-03429-z.

Supplementary Material 1.

Acknowledgements
We thank Prof. Q. Richard Lu for the gifts of *Eed*$^{flox/flox}$ mice, and thank Prof. Zhen Gu for the gifts of DC2.4 cells. We acknowledge the financial support by the National Natural Science Foundation of China (No. 82222069, 82204178, 82104181), the Zhejiang Provincial Natural Science Foundation (No. LR25H310001), the Huadong Medicine Joint Funds of the Zhejiang Provincial Natural Science Foundation of China (No. LHDMD22H310004), and the Fundamental Research Funds for the Central Universities (No. 226-2024-00094).

Author contributions
Q.J.W., J.J.W., and W.X.H. conceived and designed the study. W.X.H., H.B.M., Z.B.L., Y.W.D., W.J.X., H.Y., H.H., and Z.B.S. performed the experiments. W.X.H., H.B.M., Y.W.D., Z.B.L., H.H., and R.H.G. performed the data analysis. W.X.H., J.J.W., and Q.J.W. contributed to writing the manuscript. R.H.G., L.X.T., H.Z., J.C.W., B.Y. and Q.J.H. gave some critical advices. Q.J.W., J.J.W., H.Z., J.C.W., Q.J.H., and B.Y. contributed to the materials. All the authors read and approved the final version of the manuscript.

Availability of data and materials
The RNA-seq data of LPS or LPS + EEDi-5285 treated DC2.4 were deposited in the NCBI Gene Expression Omnibus database (accession no. GSE276064). The H3K27me3 genome binding/occupancy profiling of human DCs data downloaded and used in Fig. 4 are available in the NCBI Gene Expression Omnibus database (accession no. GSE209566).

Declarations

Consent for publication
Not applicable.

Competing interests
The authors declare no competing interests.

Received: 17 October 2024 Accepted: 25 March 2025
Published online: 01 April 2025

References:

1. Ito S, Umehara T, Koseki H. Polycomb-mediated histone modifications and gene regulation. Biochem Soc T. 2024;52:151–61.
2. Lukauskas S, Tvardovskiy A, Nguyen NV, Stadler M, Faull P, Ravnsborg T, et al. Decoding chromatin states by proteomic profiling of nucleosome readers. Nature. 2024. https://doi.org/10.1038/s41586-024-07141-5.
3. Bharti H, Han SW, Chang HW, Reinberg D. Polycomb repressive complex 2 accessory factors: rheostats for cell fate decision? Curr Opin Genet Dev 2024;84.
4. Wang JJ, Yang LJ, Dong C, Wang JC, Xu LL, Qiu YP, et al. EED-mediated histone methylation is critical for CNS myelination and remyelination by inhibiting WNT, BMP, and senescence pathways. Sci Adv. 2020. https://doi.org/10.1126/sciadv.aaz6477.
5. Wang JJ, Yang LJ, Du YW, Wang JC, Weng QJ, Liu XZ, et al. BRG1 programs PRC2-complex repression and controls oligodendrocyte differentiation and remyelination. J Cell Biol. 2024. https://doi.org/10.1083/jcb.202310143.
6. Bao QC, Kumar A, Wu DQ, Zhou J. Targeting EED as a key PRC2 complex mediator toward novel epigenetic therapeutics. Drug Discov Today 2024;29.
7. Huang Y, Sendzik M, Zhang J, Gao ZT, Sun YF, Wang L, et al. Discovery of the clinical candidate MAK683: an EED-directed, allosteric, and selective PRC2 inhibitor for the treatment of advanced malignancies. J Med Chem. 2022;65:5317–33.
8. Farias AS, Spagnol GS, Bordeaux-Rego P, Oliveira COF, Fontana AGM, de Paula RFO, et al. Vitamin D_3 induces IDO+ tolerogenic DCs and enhances treg, reducing the severity of EAE. Cns Neurosci Ther. 2013;19:269–77.
9. Jakimovski D, Bittner S, Zivadinov R, Morrow SA, Benedict RH, Zipp F, et al. Multiple sclerosis. Lancet. 2024;403:183–202.
10. Malhotra S, Villar LM, Costa C, Midaglia L, Cubedo M, Medina S, et al. Circulating EZH2-positive T cells are decreased in multiple sclerosis patients. J Neuroinflamm 2018;15.
11. Safari-Alighiarloo N, Rezaei-Tavirani M, Taghizadeh M, Tabatabaei SM, Namaki S. Network-based analysis of differentially expressed genes in cerebrospinal fluid (CSF) and blood reveals new candidate genes for multiple sclerosis. Peerj 2016;4.
12. Yang XM, Bam M, Nagarkatti PS, Nagarkatti M. Cannabidiol regulates gene expression in encephalitogenic t cells using histone methylation and noncoding RNA during experimental autoimmune encephalomyelitis. Sci Rep-Uk 2019;9.
13. Zhang XL, Wang Y, Yuan J, Li N, Pei SY, Xu J, et al. Macrophage/microglial Ezh2 facilitates autoimmune inflammation through inhibition of Socs3. J Exp Med. 2018;215:1365–82.
14. Gunawan M, Venkatesan N, Loh JT, Wong JF, Berger H, Neo WH, et al. The methyltransferase Ezh2 controls cell adhesion and migration through direct methylation of the extranuclear regulatory protein talin. Nat Immunol. 2015;16:505-U225.
15. Zhan YF, Zhang YX, Zhang SB, Coughlan H, Baldoni PL, Jacquelot N, et al. Differential requirement for the Polycomb repressor complex 2 in dendritic cell and tissue-resident myeloid cell homeostasis. Sci Immunol 2021;6.
16. Naito T, Muroi S, Taniuchi I, Kondo M. Loss of Eed leads to lineage instability and increased CD8 expression of mouse $CD4^+$ T cells upon TGFβ signaling. Mol Immunol. 2018;94:140–52.
17. Melo GA, Calôba C, Brum G, Passos TO, Martinez GJ, Pereira RM. Epigenetic regulation of T cells by Polycomb group proteins. J Leukocyte Biol. 2022;111:1253–67.
18. Yi L, Li ZQ, Hu TJ, Liu J, Li N, Cao XT, et al. Intracellular HSP70L1 inhibits human dendritic cell maturation by promoting suppressive H3K27me3 and H2AK119Ub1 histone modifications. Cell Mol Immunol. 2020;17:85–94.
19. Shao T, Ji JF, Zheng JY, Li C, Zhu LY, Fan DD, et al. Zbtb46 controls dendritic cell activation by reprogramming epigenetic regulation of *cd80/86* and *cd40* costimulatory signals in a zebrafish model. J Immunol. 2022;208:2686–701.
20. Hawiger D. Emerging T cell immunoregulatory mechanisms in multiple sclerosis and Alzheimer's disease. Front Aging Neurosci 2024;16.
21. Wang J, Wang J, Hong W, Zhang L, Song L, Shi Q, et al. Optineurin modulates the maturation of dendritic cells to regulate autoimmunity through JAK2-STAT3 signaling. Nat Commun. 2021;12:6198.
22. Alakhras NS, Kaplan MH. Dendritic cells as a nexus for the development of multiple sclerosis and models of disease. Adv Biol-Ger. 2023. https://doi.org/10.1002/adbi.202300073.
23. He YP, Selvaraju S, Curtin ML, Jakob CG, Zhu HZ, Comess KM, et al. The EED protein-protein interaction inhibitor A-395 inactivates the PRC2 complex. Nat Chem Biol. 2017;13:389.
24. Rej RK, Wang CW, Lu JF, Wang M, Petrunak E, Zawacki KP, et al. EEDi-5285: an exceptionally potent, efficacious, and orally active small-molecule inhibitor of embryonic ectoderm development. J Med Chem. 2020;63:7252–67.
25. Qi W, Zhao KH, Gu JT, Huang Y, Wang YZ, Zhang HL, et al. An allosteric PRC2 inhibitor targeting the H3K27me3 binding pocket of EED. Nat Chem Biol. 2017;13:381.
26. Liu J, Zhang X, Chen K, Cheng Y, Liu S, Xia M, et al. CCR7 chemokine receptor-inducible lnc-Dpf3 restrains dendritic cell migration by

inhibiting HIF-1alpha-mediated glycolysis. Immunity. 2019;50(600–15): e15.
27. Hong W, Yang B, He Q, Wang J, Weng Q. New insights of CCR7 signaling in dendritic cell migration and inflammatory diseases. Front Pharmacol. 2022;13: 841687.
28. Dunham I, Kundaje A, Aldred SF, Collins PJ, Davis C, Doyle F, et al. An integrated encyclopedia of DNA elements in the human genome. Nature. 2012;489:57–74.
29. Benvenuti F. The dendritic cell synapse: a life dedicated to T cell activation. Front Immunol 2016;7.
30. Al-Alwan MM, Rowden G, Lee TDG, West KA. Cutting edge: The dendritic cell cytoskeleton is critical for the formation of the immunological synapse. J Immunol. 2001;166:1452–6.
31. Al-Alwan MM, Liwski RS, Haeryfar SMM, Baldridge WH, Hoskin DW, Rowden G, et al. Cutting edge: Dendritic cell actin cytoskeletal polarization during immunological synapse formation is highly antigen-dependent. J Immunol. 2003;171:4479–83.
32. Faure-André G, Vargas P, Yuseff MI, Heuzé M, Diaz J, Lankar D, et al. Regulation of dendritic cell migration by CD74, the MHC class II-associated invariant chain. Science. 2008;322:1705–10.
33. Heras-Murillo I, Adán-Barrientos I, Galán M, Wculek SK, Sancho D. Dendritic cells as orchestrators of anticancer immunity and immunotherapy. Nat Rev Clin Oncol. 2024;21:257–77.
34. Alraies Z, Rivera CA, Delgado MG, Sanseau D, Maurin M, Amadio R, et al. Cell shape sensing licenses dendritic cells for homeostatic migration to lymph nodes. Nat Immunol 2024.
35. Clarkson BD, Walker A, Harris MG, Rayasam A, Hsu M, Sandor M, et al. CCR7 deficient inflammatory Dendritic Cells are retained in the Central Nervous System. Sci Rep-Uk. 2017. https://doi.org/10.1038/srep42856.
36. Ferrara G, Benzi A, Sturla L, Marubbi D, Frumento D, Spinelli S, et al. Sirt6 inhibition delays the onset of experimental autoimmune encephalomyelitis by reducing dendritic cell migration. J Neuroinflamm. 2020. https://doi.org/10.1186/s12974-020-01906-1.
37. Shi Y, Wang XX, Zhuang YW, Jiang Y, Melcher K, Xu HE. Structure of the PRC2 complex and application to drug discovery. Acta Pharmacol Sin. 2017;38:963–76.
38. Kim SJ, Kiser PK, Asfaha S, Dekoter RP, Dick FA. EZH2 inhibition stimulates repetitive element expression and viral mimicry in resting splenic B cells. Embo J. 2023. https://doi.org/10.15252/embj.2023114462.
39. Sun HM, Li XT, Pommer W, Xiong YQ, Chen X, Chu C, et al. GSK343 modulates macrophage M2 polarization through the EZH2/MST1/ YAP1 signaling axis to mitigate neurological damage induced by hypercalcemia in CKD mice. Cell Signal. 2024;116:111063.
40. Mei SY, Liu YH, Bao Y, Zhang Y, Min SP, Liu YF, et al. Dendritic cell-associated miRNAs are modulated via chromatin remodeling in response to different environments. PLoS ONE. 2014;9:e90231.
41. Wang JF, Iwanowycz S, Yu F, Jia XM, Leng SL, Wang YZ, et al. microRNA-155 deficiency impairs dendritic cell function in breast cancer. Oncoimmunology. 2016;5:e1232223.
42. Liu Z, Cao W, Xu LX, Chen X, Zhan Y, Yang Q, et al. The histone H3 lysine-27 demethylase Jmjd3 plays a critical role in specific regulation of Th17 cell differentiation. J Mol Cell Biol. 2015;7:505–16.
43. Doñas C, Carrasco M, Fritz M, Prado C, Tejón G, Osorio-Barrios F, et al. The histone demethylase inhibitor GSK-J4 limits inflammation through the induction of a tolerogenic phenotype on DCs. J Autoimmun. 2016;75:105–17.
44. Doñas C, Neira J, Osorio-Barrios F, Carrasco M, Fernández D, Prado C, et al. The demethylase inhibitor GSK-J4 limits inflammatory colitis by promoting de novo synthesis of retinoic acid in dendritic cells. Sci Rep-Uk. 2021. https://doi.org/10.1038/s41598-020-79122-3.
45. Huang MW, Wang Q, Long F, Di Y, Wang JH, Zhu YZ, et al. Jmjd3 regulates inflammasome activation and aggravates DSS-induced colitis in mice. Faseb J. 2020;34:4107–19.
46. Wu WJ, Qin M, Jia WW, Huang Z, Li ZZ, Yang D, et al. Cystathionine-γ-lyase ameliorates the histone demethylase JMJD3-mediated autoimmune response in rheumatoid arthritis. Cell Mol Immunol. 2019;16:694–705.
47. Zhao Z, Zhang YZ, Gao DL, Zhang YD, Han WW, Xu XM, et al. Inhibition of histone H3 lysine-27 demethylase activity relieves rheumatoid arthritis symptoms *via* repression of IL6 transcription in macrophages. Front Immunol. 2022;13:818070.
48. De Santa F, Narang V, Yap ZH, Tusi BK, Burgold T, Austenaa L, et al. Jmjd3 contributes to the control of gene expression in LPS-activated macrophages. Embo J. 2009;28:3341–52.
49. Ai SS, Peng Y, Li C, Gu F, Yu XH, Yue YZ, et al. EED orchestration of heart maturation through interaction with HDACs is H3K27me3-independent. Elife. 2017;6(6):e24570.
50. Manoharan I, Hong Y, Suryawanshi A, Angus-Hill ML, Sun ZM, Mellor AL, et al. TLR2-dependent activation of β-catenin pathway in dendritic cells induces regulatory responses and attenuates autoimmune inflammation. J Immunol. 2014;193:4203–13.
51. Manicassamy S, Reizis B, Ravindran R, Nakaya H, Salazar-Gonzalez RM, Wang YC, et al. Activation of β-catenin in dendritic cells regulates immunity versus tolerance in the intestine. Science. 2010;329:849–53.
52. Reuter S, Martin H, Beckert H, Bros M, Montermann E, Belz C, et al. The Wnt/β-catenin pathway attenuates experimental allergic airway disease. J Immunol. 2014;193:485–95.
53. Kellersch B, Brocker T. Langerhans cell homeostasis in mice is dependent on mTORC1 but not mTORC2 function. Blood. 2013;121:298–307.
54. Koppens MAJ, Bounova G, Gargiulo G, Tanger E, Janssen H, Cornelissen-Steijger P, et al. Deletion of polycomb repressive complex 2 from mouse intestine causes loss of stem cells. Gastroenterology. 2016;151:684.
55. Mirzamohammadi F, Papaioannou G, Inloes JB, Rankin EB, Xie HF, Schipani E, et al. Polycomb repressive complex 2 regulates skeletal growth by suppressing Wnt and TGF-β signalling. Nat Commun. 2016;7:12047.
56. Che J, Li D, Hong W, Wang L, Guo Y, Wu M, et al. Discovery of new macrophage M2 polarization modulators as multiple sclerosis treatment agents that enable the inflammation microenvironment remodeling. Eur J Med Chem. 2022;243:114732.

Publisher's Note